

Subproject C1.1

Synthesis and Structural Characterization of Molecule-Based Nanostructures

Principle Investigator: Dieter Fenske

CFN-Financed Scientists: Dr. Claudia Persau (1/2 BAT IIa, 48 months), Dr. Weifeng Shi (1 BAT IIa, 37 months), Dr. Jiatao Zhang (1/2 BAT IIa, 27 months), Tatjana Mitikina (1/2 BAT IIa, 12 months), Ekaterina Maynicheva (1/2 BAT IIa, 12 months), Benjamin Reiser (1/2 BAT IIa, 36 months), Robert Langer (1/2 BAT IIa, 14 months)

Further Scientists: Dr. Andreas Eichhöfer, Dr. Olaf Fuhr, Dr. Alexander Rothenberger, Dr. Heino Sommer, Dr. Stefan Wieber, Dr. Bettina Bechlars

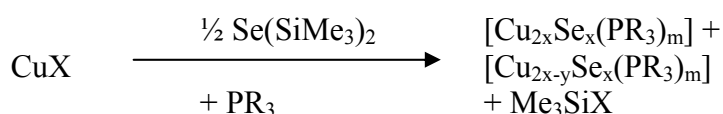
**Institut für Anorganische Chemie
Universität Karlsruhe (TH)**

**Institut für Nanotechnologie
Forschungszentrum Karlsruhe in der Helmholtz-Gemeinschaft**

C1.1 Synthesis and Characterization of Molecule based Nanostructures (D. Fenske, A. Eichhöfer, O. Fuhr, A. Rothenberger)

1 Selenido- and Selenolato-bridged Copper clusters

Since several years we have now investigated reactions of copper salts with $\text{Se}(\text{SiMe}_3)_2$ and RSeSiMe_3 (R = organic group) which lead in the presence of monodentate and bidentate phosphine ligands to the formation of ligand stabilized $[\text{Cu}_{2n}\text{Se}_n]$ -cluster molecules [1]. These compounds are stabilized kinetically. Therefore they tend to decompose and to form the stable binary phase Cu_2Se . Important for the structures of the so formed clusters are the reaction conditions like the solvent, the reaction temperature, the stoichiometry of the precursor compounds, the kind of the anion X in the copper salt and the organic groups of the phosphine ligands.



X : halogenide, acetate, pseudo halogenide

Scheme 1

The copper chalcogenide cluster cores can adopt a composition which is different from the ideal copper : chalcogen ratio (2 : 1) in the bulk phase Cu_2Se . The following compounds have been synthesized and characterized earlier [1]:

$[\text{Cu}_{12}\text{Se}_6(\text{PR}_3)_8]$ (R = Et_2Ph , $n\text{Pr}_3$ oder Cy), $[\text{Cu}_{20}\text{Se}_{13}(\text{PET}_3)_{12}]$, $[\text{Cu}_{29}\text{Se}_{15}(\text{PiPr}_3)_{12}]$, $[\text{Cu}_{30}\text{Se}_{15}(\text{PR}_3)_{12}]$ (R = $i\text{Pr}_3$ oder $t\text{Bu}_2\text{Me}$), $[\text{Cu}_{31}\text{Se}_{15}(\text{SeSiMe}_3)(\text{PtBu}_2\text{Me})_{12}]$, $[\text{Cu}_{36}\text{Se}_{18}(\text{PtBu}_3)_{12}]$, $[\text{Cu}_{44}\text{Se}_{22}(\text{PET}_2\text{Ph})_{18}]$, $[\text{Cu}_{44}\text{Se}_{22}(\text{PnBu}_t\text{Bu}_2)_{12}]$, $[\text{Cu}_{48}\text{Se}_{24}(\text{PMe}_2\text{Ph})_{20}]$, $[\text{Cu}_{70}\text{Se}_{35}(\text{PET}_3)_{22}]$, $[\text{Cu}_{70}\text{Se}_{35}(\text{PiPr}_2\text{Me})_{21}]$, $[\text{Cu}_{70}\text{Se}_{35}(\text{PtBu}_2\text{Me})_{21}]$ and $[\text{Cu}_{146}\text{Se}_{73}(\text{PPh}_3)_{30}]$.

In order to get a better understanding of the process of the formation of intermediates in the cluster synthesis further attempts in the characterization of new cluster molecules were undertaken. The following intermediates have been successfully isolated.



In addition some selenido-selenolato bridged complexes like $[\text{Cu}_{32}\text{Se}_7(\text{SenBu})_{18}(\text{PiPr}_3)_6]$ (6), $[\text{Cu}_{50}\text{Se}_{20}(\text{SetBu})_{10}(\text{PiPr}_3)_{10}]$ (7) and $\text{Cu}_{73}\text{Se}_{35}(\text{SePh})_3(\text{PiPr}_3)_{21}$ (8) were also synthesized.

1–8 are molecular cluster molecules with the copper atoms formally in the oxidation state +I. Up to a size of 68 copper atoms the structures have no similarity with the solid state structures of the binary copper chalcogenides. This changes suddenly when the cluster contains 70 and more copper atoms. Then one can find disk like triangular molecules with the chalcogenide atoms forming a three dimensional network similar to a hexagonal closed packing. The copper atoms reside in the tetrahedral holes.

In $[\text{Cu}_{140}\text{Se}_{70}(\text{PET}_3)_{34}]$ there are three parallel layers consisting of 21, 28 and 21 selenium atoms. Contrasting in $[\text{Cu}_{146}\text{Se}_{73}(\text{PPh}_3)_{30}]$ the middle layer is formed by 31 selenium atoms.

Therefore the transition from 4 and 5 to the structure of the Cu_{146} cluster is a topological analogon to the change observed regarding the selenium networks in $[\text{Cu}_{70}\text{Se}_{35}(\text{PET}_3)_{22}]$ and $[\text{Cu}_{74}\text{Se}_{38}(\text{PCy}_3)_{18}]$. Due to these observations one might conclude that the structures of the 'larger' $[\text{Cu}_2\text{Se}]$ -clusters are determined by so called "magic numbers" which also determine the

composition. Table 1 lists compositions of known and hypothetical Cu_2Se -cluster which could exist due to this concept of „magic numbers“.

formula (without PR_3)	Se-atoms in the		
	1. layer	2. layer	3. layer
$\text{Cu}_{70}\text{Se}_{35}$	10	15	10
$\text{Cu}_{74}\text{Se}_{38}$	10	18	10
$\text{Cu}_{102}\text{Se}_{51}$	15	21	15
$\text{Cu}_{140}\text{Se}_{70}$	21	28	21
$\text{Cu}_{146}\text{Se}_{73}$	21	31	21
$\text{Cu}_{184}\text{Se}_{92}$	28	36	28
$\text{Cu}_{234}\text{Se}_{117}$	36	45	36
$\text{Cu}_{290}\text{Se}_{145}$	45	55	45
$\text{Cu}_{354}\text{Se}_{177}$	55	67	55
$\text{Cu}_{428}\text{Se}_{214}$	67	80	67

Table 1. Composition of selenium layers in known and *hypothetical* $[\text{Cu}_2\text{Se}]$ -cluster molecules.

In agreement with these consideration we recently were able to prove in the compound $[\text{Cu}_{93}\text{Se}_{42}(\text{Se}-\text{C}_6\text{H}_4-\text{SMe})_9(\text{PPh}_3)_{18}]$ a network which is composed by 51 selenium and thus is an intermediate between the Cu_{74} and the Cu_{140} Cluster [2]. The structure is displayed in Figure 1.

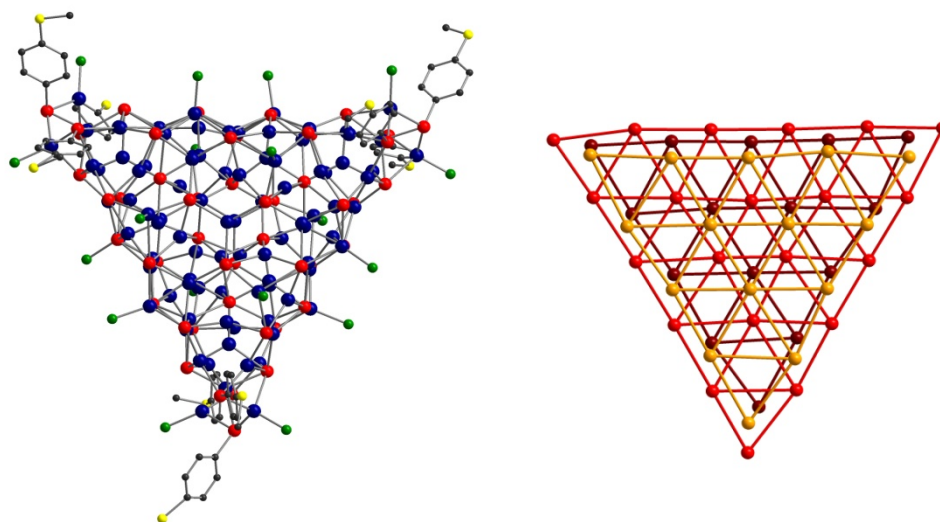


Figure 1. *left:* molecular structure of $[\text{Cu}_{93}\text{Se}_{42}(\text{Se}-\text{C}_6\text{H}_4-\text{SMe})_9(\text{PPh}_3)_{18}]$ (Cu: blue, Se: red, P: green, S: yellow; C atoms of PPh_3 omitted); *right:* selenium substructure.

Evidences for the existence of these larger copper selenide clusters have been found in mass spectra. MALDI-TOF-spectra prove the existence of $[(\text{Cu}_2\text{Se})_n]^+$ -cations with a molecular weight up to 500000 Da.

Although numerous attempts to isolate and characterize further intermediate products on the way to the formation of very large cluster complexes have been unsuccessful, up to now their existence is still thinkable. In order to synthesize cluster molecules of the composition $[(\text{Cu}_2\text{Se})_n(\text{PR}_3)_m]$ ($n > 73$) the steric demand of the phosphine ligands has to be changed. This could lead to larger selenium networks. Obviously the disk-like structures in **3**, **4**, **5** and **8** have remarkable low surface energies which may favour these compositions. Further cluster growth could then result in a lateral extension

of the three selenium layers. At the same time growth of the clusters could also result in an enlargement of the numbers of layers which would in the end lead to a cubic closed packing of selenium atoms similar to what is found for the high temperature phase of Cu_2Se . As already described the copper clusters discussed are kinetically stabilized molecules. Quantum chemical calculations reveal that the Cu-P-bonding energy in the larger clusters represents only a few $\text{kJ}\cdot\text{mol}^{-1}$. This is the reason why the phosphine ligands can be cleaved at ambient temperatures. The thermal decomposition yields metastable Cu_2Se which converts at $210\text{ }^\circ\text{C}$ to form $\alpha\text{-Cu}_2\text{Se}$.



Scheme 2

Cleavage temperatures are found to depend both on the cluster size and the kind of phosphine ligand. The particle size of the so formed Cu_2Se -particles depends on the other hand on the size of the precursor cluster and on temperature. The edge length of the triangular $[\text{Cu}_{70}\text{Se}_{35}]$ -cluster core of the precursor cluster $[\text{Cu}_{70}\text{Se}_{35}(\text{PET}_3)_{22}]$ is 1.7 nm. One can assume that at low temperatures under vacuum conditions only the PET_3 ligands are removed from the cluster surface. This should lead to the formation of ligand free $[\text{Cu}_2\text{Se}]$ -nanoparticles with comparable edge lengths. This assumption is confirmed by particle size determinations via powder diffractometry and electron microscopy. In this way it should be also possible to synthesize Cu_2Se particles of different sizes by using phosphine stabilized copper selenide clusters of different size.

An increase of the cleavage temperature results in an increase of the resulting particle sizes. The following temperature dependence of the resulting particle size is recorded for $[\text{Cu}_{70}\text{Se}_{35}(\text{PET}_3)_{22}]$:

T/ $^\circ\text{C}$	100	130	200	600
Mean particle size/nm	1.7	12.4	18.2	740

The thermal cleavage of the tertiary phosphine ligands can also be achieved inside electrochemically fabricated Al_2O_3 -membranes. The empty nanotubes (mean diameter 30 – 100 nm) of the membrane are filled with cluster molecules by dipping them into solutions of $[\text{Cu}_{70}\text{Se}_{35}(\text{PET}_3)_{22}]$. The PET_3 ligands can be cleaved at temperatures around $300\text{ }^\circ\text{C}$ but as a consequence of the use of higher temperatures the smaller $[\text{Cu}_{70}\text{Se}_{35}]$ -nanocluster which are originally formed at lower temperatures tend to aggregate in order to form larger particles. Interestingly these particles display now the triangular structure of the precursor cluster. Due to Figure 2 the TEM images reveal that these larger clusters form agglomerates of triangles in the membrane.

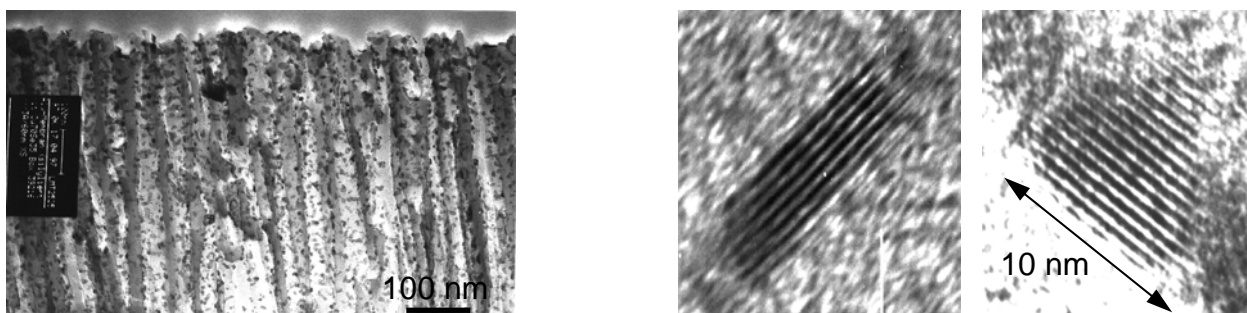


Figure 2: *left*: TEM-image of Al_2O_3 -nanotubes filled with $[\text{Cu}_2\text{Se}]_x$ -cluster; *right*: TEM-images of a $[\text{Cu}_2\text{Se}]_x$ nanoclusters in different orientations.

On the right hand side of Figure 2 one of these triangular nanoparticles is mapped in a higher resolution. It is shown that under the given conditions particles are formed with an edge length of 10 nm which do not only show a lateral growth but also increased in thickness by a factor of 2-3 compared with the precursor cluster molecules. The distance of the lattice planes is about 0.68 nm. These experiments show that it is under these conditions ($T > 210\text{ }^{\circ}\text{C}$) possible to form very large copper selenide nanoparticles which possess the $\alpha\text{-Cu}_2\text{Se}$ structure with a particle size depending on the decomposition temperature.

We have now investigated the properties of further phosphine stabilized cluster molecules. For this purpose cluster complexes with different phosphine ligands have been synthesized. [3] The reaction of CuX ($\text{X} = \text{Cl}, \text{OOCCH}_3$) with PEt_2Ph or PEt_3 and $\text{Se}(\text{SiMe}_3)_2$ in organic solvents results in the formation of crystals of two series of copper selenide cluster molecules namely $[\text{Cu}_{26}\text{Se}_{13}(\text{PEt}_2\text{R})_{14}]$ ($\text{R} = \text{Ph}$ (**9**), Et (**10**)), $[\text{Cu}_{44}\text{Se}_{22}(\text{PEt}_2\text{Ph})_{18}]$ (**11**), $[\text{Cu}_{70}\text{Se}_{35}(\text{PEt}_2\text{R})_{23}]$ ($\text{R} = \text{Ph}$ (**12**), Et (**13**)) and $[\text{Cu}_{140}\text{Se}_{70}(\text{PEt}_3)_{34}]$ (**14**).

For all compounds the crystal structures have been determined by single crystal X-ray analysis representing in four different types of copper selenide cluster cores

Thermal Properties of 9–14

The investigations of the thermal properties of **9–14** are focused on the cleavage behaviour of the phosphine ligands along with their cleavage temperatures under different experimental conditions and the characterisation of the residues. Therefore the thermogravimetric analyses of **9**, **11**, **12** and **10**, **13**, **14** were measured in vacuum and in an inert gas flow of helium. Simultaneously recorded mass spectra of the volatile products of **10**, **13** and **14** confirm that PEt_3 is liberated, while the dominant peaks in mass in the spectra of **9**, **11** and **12** are located at the expected positions for PEt_2Ph and its fragmentation products. These results suggest in all cases the formation of Cu_2Se , which was proven by powder diffractometry for all compounds and by elemental analysis.

Apart from these obvious observations the different onsets and temperature ranges of the TGA of **9–14** in either helium gas flow or vacuum atmosphere suggest complex processes and influencing parameters which are difficult to discuss. The onset temperature of the cleavage process is generally reduced upon the use of vacuum instead of helium gas flow by 20–50 $^{\circ}\text{C}$ along with a visible reduction of the temperature range of the decomposition by approximately 30–60 $^{\circ}\text{C}$ for all compounds. With respect to the different kind of phosphine ligand the mean cleavage temperatures in vacuum are found to be significantly lower for **10** and **13** ligated by PEt_3 than observed for the similarly sized clusters **9**, **11** and **12** which are coordinated by PEt_2Ph . One explanation for this increase in temperature could be a stronger Cu-P bonding for PEt_2Ph instead of PEt_3 , but more likely this behaviour originates from the different boiling points of PEt_3 (126–128 $^{\circ}\text{C}$) and PEt_2Ph (222 $^{\circ}\text{C}$). However the mean temperatures of the TGA curves measured with helium gas flow do not, with the exception of **10**, show such a phosphine dependent difference.

For **10**, **13** and **14**, which are coordinated by the lower boiling PEt_3 one observes additionally under vacuum atmosphere a distinct dependence of the mean cleavage temperature on the size of the cluster such that it increases with increasing cluster size. A similar behaviour is also observed for for the PEt_3 ligated cluster molecules measured under a helium gas flow. Assuming that these effects are not governed by the size and quality of the crystals of the precursor complexes this fact might be explained in two ways. On the one hand this could mean that larger clusters induce a stronger bonding of the phosphine to the cluster core. This contrasts, however, with DFT calculations of Ahlrichs et al. who found that for copper selenide cluster molecules a decrease in the Cu-P binding energy upon going from smaller to larger clusters is expected.

Solid state ^{31}P -NMR signals of the clusters coordinated by PEt_2Ph **9** (–21.9 ppm), **11** (–17.9 ppm) and **12** (–15.6 ppm) as well as those ligated by PEt_3 **10** (–26.1 ppm) and **13** (–17.7 ppm) indicate

decreased shielding of the phosphorous nuclei with increasing cluster size (table 3). However this gives no clear information about the strength of the Cu–P bond as it can be interpreted either by a stronger dative P→Cu bonding or a weakening of the Cu→P back bonding in the larger cluster molecules. On the other hand further calculations reveal that the stability of these types of clusters should increase with increasing cluster size, which means that the tendency to form the bulk material decreases in the same direction.

Powder X-ray diffraction patterns of the black residues reveal the formation of Cu₂Se for all compounds **9–14**. The d-values of the powder patterns of the black residues at the end of the cleavage process for all clusters are in good agreement with those found for monoclinic α-Cu₂Se (Figure 3).

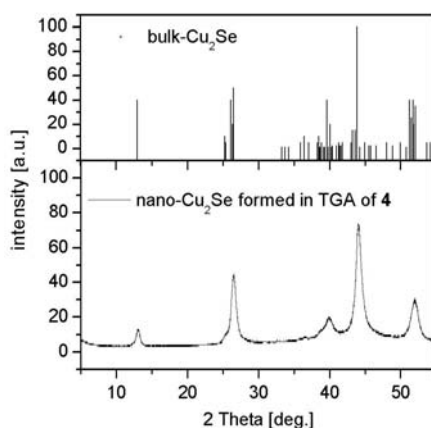


Figure 3. X-ray powder diffraction pattern of the black residue of the thermogravimetical analysis of [Cu₇₀Se₃₅(PEt₂Ph)₂₃] (**12**) in vacuum (lower graph) and of monoclinic α-Cu₂Se (upper graph).

The relative broadness of the diffraction peaks indicates a nanostructuring of the material. For Cu₂Se only the peak at 2Θ = 13 ° is suitable for this analysis as literature data reveal that the other peaks which are apparently single consists of several reflections. The calculated mean particle size *D* yielded values between 12 and 16 nm for Cu₂Se powders resulting from a thermal treatment of **9–14** in vacuum up to 150 °C (Table 2). The cluster cores of **9–14** have edge lengths of 0.8–1.5 nm which reveals a distinct growth of the precursor cluster molecules with the cleavage of the phosphine ligands. The differences in size are difficult to explain and show no obvious relation to the size of the precursor cluster but could also result from a difference in size and quality of the precursor crystals. Sintering of the samples at 150 °C for five hours does not lead to a significant increase in particle size. However the size of the crystalline domains doubles when the samples were heated to final temperature of 300 °C.

Compound	estimated particle sizes [nm]		
	150 °C	150 °C + 5h of sintering	300 °C
[Cu ₂₆ Se ₁₃ (PEt ₂ Ph) ₁₄] (9)	15	15	34
[Cu ₄₄ Se ₂₂ (PEt ₂ Ph) ₁₈] (11)	13	14	34
[Cu ₇₀ Se ₃₅ (PEt ₂ Ph) ₂₃] (12)	14	13	32
[Cu ₂₆ Se ₁₃ (PEt ₃) ₁₄] (10)	12	14	30
[Cu ₇₀ Se ₃₅ (PEt ₃) ₂₃] (13)	16	15	30
[Cu ₁₄₀ Se ₇₀ (PEt ₃) ₃₄] (14)	12	14	32

Table 2. : Estimated crystallite sizes (Scherrer equation) for the Cu₂Se powders which result from the thermal decomposition of **9–14** at 150 °C and 300 °C.

TEM measurements of the nanostructured Cu₂Se powders as a suspension in THF did not give any valuable structural information due to the relative thickness of the material resulting from

agglomeration on the grids. Thus, the thermally treated brittle crystals were embedded in resin and subsequently cut by a microtom. Figure 4 shows a small, but representative sample section of a crystal of **12** heated to 150 °C in vacuum with two intergrown crystalline domains of copper selenide with domain sizes of roughly 15 nm.

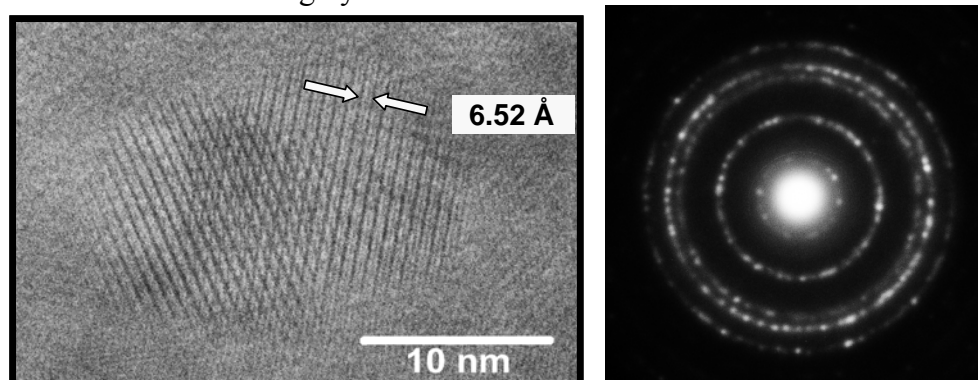


Figure 4. *left:* Section of a HRTEM photograph of a microtom slice of a crystal of thermally treated $[\text{Cu}_{70}\text{Se}_{35}(\text{PEt}_2\text{Ph})_{23}]$ (**12**); *right:* Corresponding selected electron diffraction pattern.

In order to determine the electronic properties especially the HOMO-LUMO gaps UV-VIS spectra have been measured for some of the copper selenide cluster molecules namely $[\text{Cu}_{26}\text{Se}_{13}(\text{PEt}_2\text{Ph})_{14}]$ (**9**), $[\text{Cu}_{44}\text{Se}_{22}(\text{PEt}_2\text{Ph})_{18}]$ (**11**), $[\text{Cu}_{70}\text{Se}_{35}(\text{PEt}_2\text{Ph})_{24}]$ (**12**) and $[\text{Cu}_{146}\text{Se}_{73}(\text{PPh}_3)_{30}]$ (Figure 5). The size of the $[\text{Cu}_2\text{Se}]$ -core ranges from 1.1 nm for the Cu_{26} -Cluster to 1.3 nm (Cu_{44}), 1.7 nm (Cu_{70}) and 2.6 nm for the largest Cu_{146} cluster molecule. The spectra reveal a decrease of the HOMO-LUMO gap on going from the smallest cluster **9** with a HOMO-LUMO gap of 1.94 eV to an energy of 1.3 eV in $[\text{Cu}_{146}\text{Se}_{73}(\text{PPh}_3)_{30}]$ which is already close to the largest of the experimental values for the band gap in Cu_2Se which vary from 1.1 eV (1127 nm) from optical measurements to 0.37 eV (3350 nm) from electrochemical measurements. The increase of the HOMO-LUMO gap with reduction in particle size is similar to the behaviour of CdSe and CdS nanoparticles showing the so called quantum size effect.

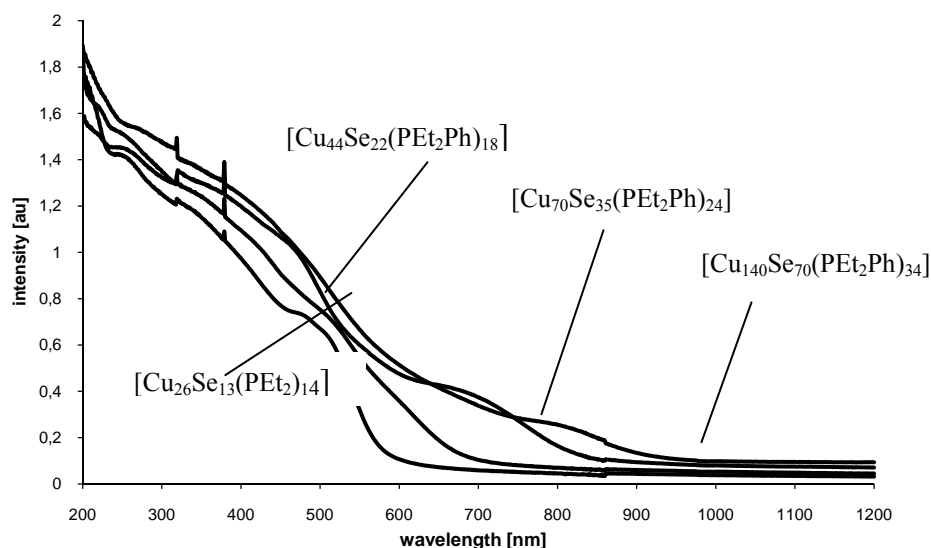


Figure 5. : UV-VIS-spectra (solid state) of different copper selenide cluster molecules.

In this context it is not surprising that the photoluminescence of the differently sized $[\text{Cu}_2\text{Se}]$ -cluster molecules is also influenced by the particle size. This becomes obvious comparing the PL-spectra of $[\text{Cu}_{26}\text{Se}_{13}(\text{PEt}_2\text{Ph})_{14}]$ (**9**), $[\text{Cu}_{44}\text{Se}_{22}(\text{PEt}_2\text{Ph})_{18}]$ (**11**) and $[\text{Cu}_{70}\text{Se}_{35}(\text{PEt}_2\text{Ph})_{24}]$ (**12**) (Figure 6). In

all compounds one detects a distinct increase in the quantum yield upon lowering the measuring temperature.

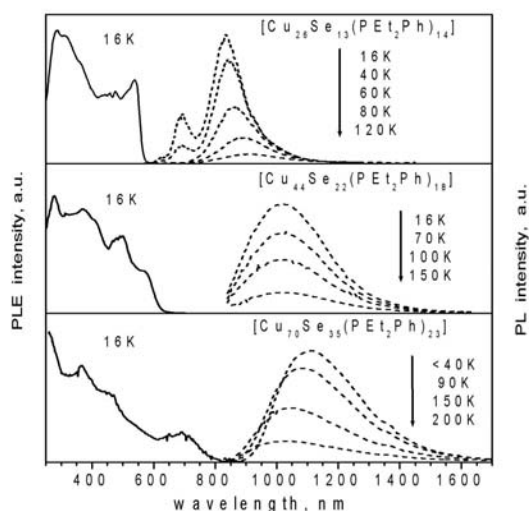
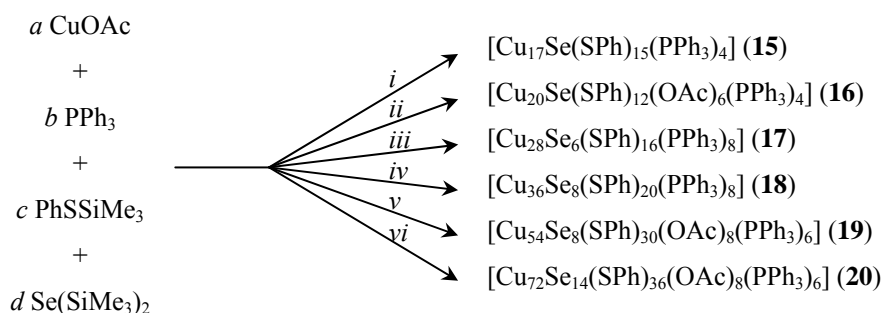


Figure 6. PL- and PLE-spectra of differently sized $[\text{Cu}_2\text{Se}]$ -cluster molecules at different temperatures.

2 Copper Chalcogenide Clusters with Selenide Core and a Sulfide Shell [4]

We were also interested in the preparation and the optical properties of core-shell particles. Therefore we synthesised a series of clusters consisting of a copper selenide core surrounded by a shell of copper sulphide.

The reactions of copper(I) acetate with a mixture of the disilylated selenium compound $\text{Se}(\text{SiMe}_3)_2$ and the monosilylated sulfur species PhSSiMe_3 lead to the formation of several new copper chalcogenide clusters. Scheme 3 summarizes the reactions leading to compounds **15-20**.



Scheme 3. : Reactions leading to compounds 15-20; ratios of the coefficients a:b:c:d i) 20:10:15:1, ii) 24:8:12:1, iii) 30:25:16:5, iv) 10:10:5:2, v) 60:15:30:5, iv) 40:10:18:7.

All compounds were crystallized and their structure determined by single-crystal X-ray analysis. Figure 7 shows the structures of the cluster core and two projections of the chalcogenide substructure of **19**.

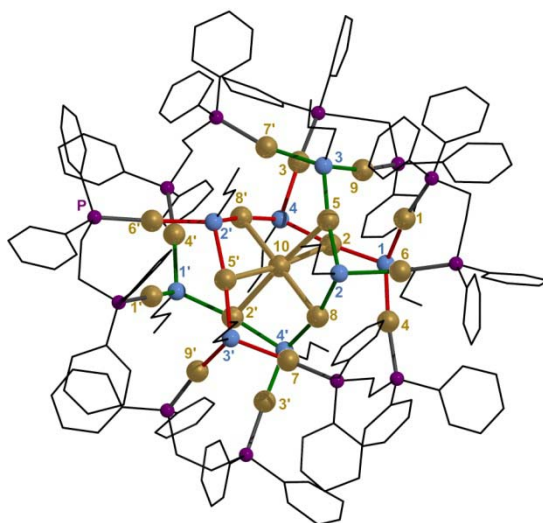


Figure 8. Molecular structures of the cations in **21**. For clarity atoms are only numbered; Au gold, As blue, P violet; organic groups represented with blacksticks.

The positive-ion Fourier transform mass spectrum obtained upon electrospraying a CH_2Cl_2 solution of **21** shown in Figure 9. The main peak V can be unambiguously assigned to the triply charged cluster ion $[\text{Au}_{19}(\text{AsnPr})_8(\text{dppe})_6]^{3+}$ in **21** on the basis of the m/z value and the highly resolved isotope splitting (Figure 19, inset). Peak VI also stems from **21**: it results from the association of one Cl^- counterion to the trication (such ion-pair formation is common in ESI-MS).

A new structural feature is found in **21**: a centered octahedron of seven gold atoms (figure 17). Compound **21** crystallizes in the tetragonal space group $P4_2/nbc$ with twelve formula units per unit cell. The asymmetric unit comprises one half and one quarter of two molecules (I and II), which occupy two different crystallographic positions (with site symmetries C_2 and D_2). The two molecules have identical compositions and slightly different structural parameters.

The trications of **21** consist of two helically arranged U-shaped Au_9As_4 chains, which are each built up from four corner-sharing Au_3As tetrahedra. The six gold atoms at the shared corners in the two chains form a distorted octahedron, which contains Au_{10} at its center. Interactions between the central atom and the vertex atoms lead to two very short distances ($\text{Au}_{10}\text{-Au}_8$) and four longer ones ($\text{Au}_{10}\text{-Au}_5$ and $\text{Au}_{10}\text{-Au}_2$). The angles between the gold atoms in the octahedron range from $66.88(3)$ – $116.13(7)^\circ$ (cis) and from $173.67(4)$ – $175.82(9)^\circ$ (trans). The resulting Au-Au edge distances, which are larger than 316.3 pm, indicate weak aureophilic interactions.

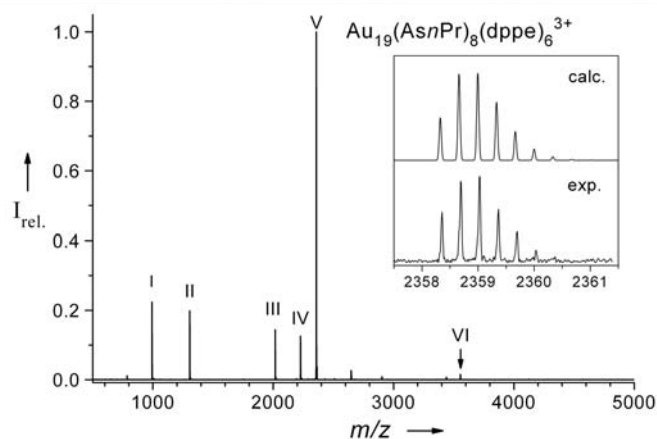


Figure 9. ESI mass spectrum (positive-ion mode) of **21** in CH_2Cl_2 . Inset: comparison of the calculated isotope splitting of the $[\text{Au}_{19}(\text{AsnPr})_8(\text{dppe})_6]^{3+}$ ion and the observed isotope splitting of peak V.

To clarify both the composition and the charge of the $[\text{Au}_{19}(\text{AsnPr})_8(\text{dppe})_6]^{3+}$ ion in **21**, DFT calculations were undertaken, prior to the ESI-MS characterization. For the cluster in **21**, three model compounds **21a–c** of formula $[\text{XAu}_{18}(\text{AsnPr})_8\{\text{Me}_2\text{P}(\text{CH}_2)_2\text{PMe}_2\}_6]^q$, where X is the atom in position Au10, and q is the ion charge, were considered and structurally optimized.



On the basis of the calculated bond lengths, we prefer model **21a**, but cannot definitely exclude **21b**. Whether X=As or Au is present as the central atom in the cation of **21** can only be decided by ESI-MS. Further support for the assignment of X=Au in the cation of **21** is provided by the comparison of the calculated electronic energies of **21a** with photoluminescence data for **21**.

4 Ternary Copper Chalcogenide Clusters

4.1 Copper-Indium Chalcogenides [12, 13]

For the synthesis of this class of compounds we used the reaction of CuCl, InCl₃ and PhSeSiMe₃, in the presence of [AsPh₄Cl]. This results in the formation of either (AsPh₄)₂[Cu₆In₄Cl₄(SePh)₁₆] (**25**) and (AsPh₄)₂[Cu₇In₄(SePh)₂₀] (**26**). The tetrahedrally shaped core of the cluster anion in **25** (figure 22) is composed of four fused distorted {InCu₃Se₆} adamantoid cages. The so-formed tetrahedral cluster cage is isostructural to known binary and ternary cluster molecules like [Cd₁₀(SCH₂CH₂OH)₁₆]⁴⁺. [14]

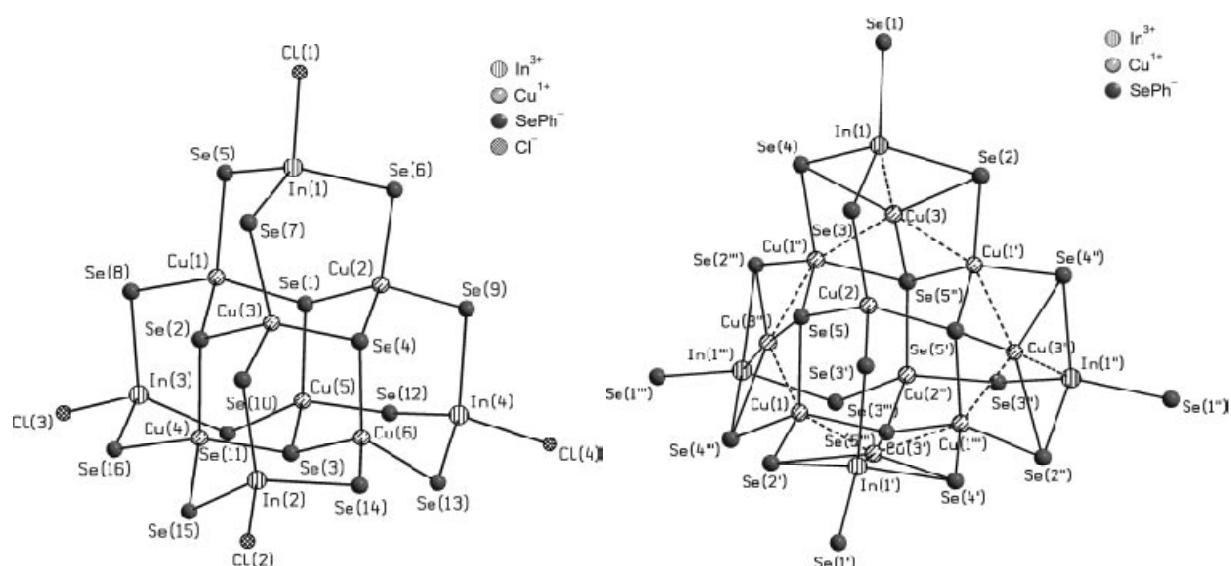


Figure 10. Molecular structure of the $[\text{Cu}_6\text{In}_4\text{Cl}_4(\text{SePh})_{16}]^{2-}$ anion in **25** (left) and of the $[\text{Cu}_7\text{In}_4(\text{SePh})_{20}]^-$ anion in **26** (right). C and H atoms are omitted.

The molecular structure of the anion core in **26**, $[\text{Cu}_7\text{In}_4(\text{SePh})_{20}]^-$ (Figure 10, right), is, with the exception of two differences, very similar to the structure of **25** (Figure 10, left). First, the use of an

excess of PhSeSiMe_3 leads to an exchange of the terminal chloro ligands with SePh^- groups. The second, and more remarkable, difference concerns the stoichiometry and charge of the cluster anion. Compared to the cluster anion of **25**, this results in a reduction of the overall charge of the cluster anion from -2 to -1 if we assign the metal atoms as In^{3+} and Cu^+ . In agreement with this, we found only one tetraphenylarsonium countercation in the crystal structure. In order to maintain the overall charge of the cluster at -1 , the electronic structure of the cluster must be significantly altered. Mass spectrometry and DFT computations were performed to address this problem.

The solid-state UV/Vis spectra of **25** and **26** (Figure 11, *bottom*) are quite similar, with a first shoulder at 400 nm (3.1 eV) and a broad maximum at 310 nm (4.0 eV). In solution, one observes similar absorption features with the bands shifted to 370 nm (3.4 eV) and 265 nm (4.7 eV), respectively. As mass spectrometry indicates the existence of the intact cluster anions in solution, the shift between solid-state and solution spectra likely arises from inhomogeneities of the crystal-oil mull between the quartz plates, which has been observed for other samples.

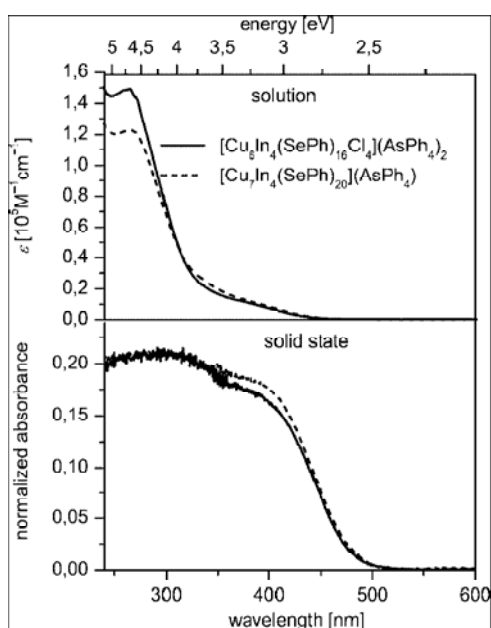


Figure 11. UV/Vis spectra of $(\text{AsPh}_4)_2[\text{Cu}_6\text{In}_4\text{Cl}_4(\text{SePh})_{16}]$ (**25**) and $(\text{AsPh}_4)[\text{Cu}_7\text{In}_4(\text{SePh})_{20}]$ (**26**) in solution (CH_2Cl_2) and in solid state.

Mass Spectrometry

The negative-ion mass spectrum of **26** (Figure 12) is governed by several strong ion signals which are all singly charged and can be clearly assigned as indicated in the graphic. The highest mass peak observed ($m/z \approx 4025$) is in complete agreement with the expected isotopomer distribution of the singly charged cluster anion $[\text{Cu}_7\text{In}_4(\text{SePh})_{20}]^-$, as can be seen from the inset in figure 25. Interestingly, the observed fragment ions differ significantly from the ion signals obtained by direct spraying of **26**.

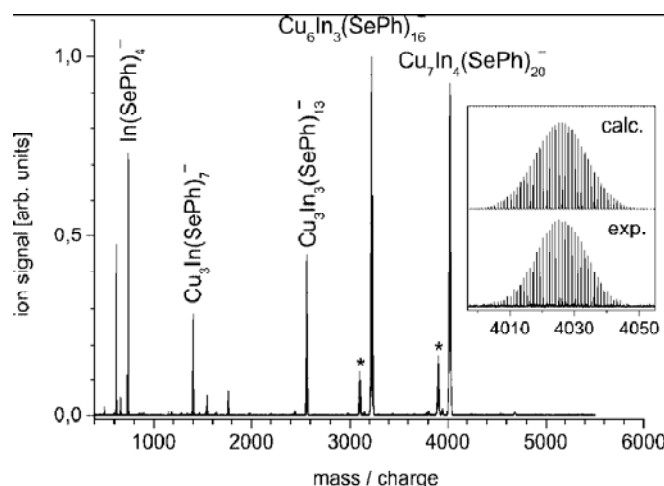


Figure 12. Negative-ion electrospray mass spectrum of 26. The inset shows a high-resolution mass spectrum of the ion peak at $m/z \approx 4025$ displaying the isotopomer splitting in comparison to the calculated distribution expected for $[\text{Cu}_7\text{In}_4(\text{SePh})_{20}]^-$.

DFT Calculations

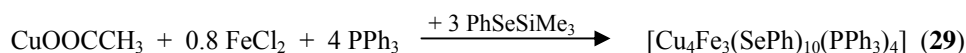
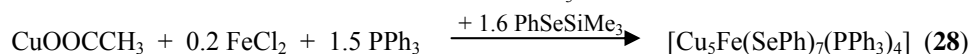
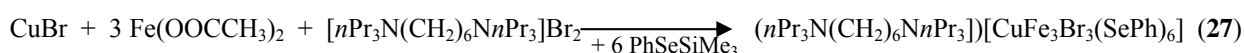
For the Cu_7 compound, the X-ray structure has some ambiguities in assignment. The crystallographically imposed $\bar{4}$ symmetry distributes the effective electron density of the seventh copper atom over four identical sites, but the observed density could conceivably be due to four fulloccupancy oxygen atoms. There should be, however, significant structural differences between the postulated Cu_7 and Cu_6O_4 cluster cores due to the vastly different electronic structure needed to maintain the 1- overall cluster charge. Density functional theory has been successfully applied to similar cluster compounds,[15] and should allow us to differentiate between these two putative assignments, as well as confirming that either are physically reasonable. The Cu_6O_4 case was quickly eliminated as it was highly unstable to geometry optimization and the electronic structure indicated a highly paramagnetic system, with essentially no HOMO–LUMO gap, contradicting the observed pale yellow color of the compound. The Cu_7 system was not, however, obviously the correct assignment. If addition of the seventh copper atom altered the rest of the cluster significantly from S_4 symmetry, the compound would be strongly disfavored from crystallizing in the observed space group. Initial geometry optimization of the $[\text{Cu}_7\text{In}_4(\text{SeR})_{20}]^-$ anion was simplified by replacing the phenyl rings of the selenium ligands with methyl groups. Addition of a Cu^+ ion to one of the adamantoid faces caused strong deviations in the geometry, the seventh copper atom having burrowed into the cluster, resulting in a related structure with C_2 symmetry. Geometry optimization of the fully phenylselenolateligated cluster proceeded successfully, with the extra copper atom remaining in the center of an external adamantoid face, and no major changes when compared to the crystal structure.

To test the assumption that the observed crystal structure is indeed the superposition of four orientations of $[\text{Cu}_7\text{In}_4(\text{SePh})_{20}]^-$, the DFT structure must be symmetrized under S_4 before comparison to experiment. The symmetrization procedure produced an averaged structure almost identical to that from the crystal, with an RMS distance of 13.7 pm between corresponding atoms in the superimposed structures, and well within the expected thermal motion. Calculated bonds in the cluster core tend to be consistently slightly longer than their respective distances in the crystal, as is expected when comparing gas-phase to solid-state structures. The final electronic structure (diamagnetic, HOMO–LUMO gap = 1.7 eV) is also in agreement with observations.

4.2 Copper Iron Chalcogenides [13]

We also tried to synthesize mixed copper iron chalcogenide clusters. These compounds could be used as starting material for CuFeS_2 , which is known as a semiconductor material. Until now only a limited number of cluster compounds have been synthesized containing Cu, Fe and a chalcogenide examples are: $[\text{Fe}_3\text{Cu}(\text{SiPr})_6\text{Cl}_3]^{2-}$ and $[\text{Fe}_2\text{Cu}_4(\text{SiPr})_8\text{Cl}_3]^{2-}$. [16].

The reaction of a 1:3 mixture of CuBr and $\text{Fe}(\text{OOCCH}_3)_2$ with PhSeSiMe_3 in acetonitrile in the presence of the diammonium salt $[\text{nPr}_3\text{N}(\text{CH}_2)_6\text{NnPr}_3]\text{Br}_2$ yielded, after layering with diethyl ether, dark red-orange crystals of **27** after a few days. The use of the neutral ligand PPh_3 instead of the diammonium salt $[\text{nPr}_3\text{N}(\text{CH}_2)_6\text{NnPr}_3]\text{Br}_2$ in reactions of CuOOCCH_3 and FeCl_2 with PhSeSiMe_3 led to the formation of dark-red solutions from which red crystals of **28** grew over the course of several days. A similar reaction with a 1:0.8 ratio of CuOOCCH_3 and FeCl_2 yielded red-orange crystals of **29**.



Scheme 5. Synthesis of 27 to 29.

The cluster anion $[\text{CuFe}_3\text{Br}_3(\text{SePh})_6]^{2-}$ in **27** (figure 27, *left*) consists of a six-membered $\text{Fe}_3(\text{SePh})_3$ ring in a chair conformation that is capped by a nearly trigonal-planar $\text{Cu}(\text{SePh})_3$ unit. Each of the iron atoms is additionally coordinated by a terminal bromido ligand to give a distorted tetrahedral coordination environment for the iron atoms. The metal–selenium distances are found to be longer for iron [246.7–246.8(2) pm] than for copper [234.2–234.3(1) pm], which is most probably a result of the different coordination modes. This adamantoid cluster core in **27** is therefore similar to the structures of $[\text{CuFe}_3\text{Cl}_3(\text{EiPr})_6]^{2-}$ (E = Se, S). [17]

The structure of **28** (Figure 13, *middle*) comprises a central Cu_3Fe trigonal pyramid formed by Cu(1), Cu(2), Cu(3), and Fe(1) with the six edges bridged by SePh^- . One additional copper atom [Cu(4)] is bonded to this adamantoid cluster cage through the three selenium atoms of the basal six-membered ring. The coordination environment of Cu(4) is trigonal-planar. The copper atoms Cu(1)–Cu(3) which form the basal plane of the Cu_3Fe pyramid are each additionally coordinated by a terminal PPh_3 ligand to result in an overall distorted tetrahedral coordination environment for these atoms. Fe(1), at the apex of the Cu_3Fe pyramid, is additionally coordinated by another SePh^- ligand [Se(7)], and a further CuPPh_3 unit is attached through this and two other SePh^- ligands [Se(5), Se(6), Se(7)] to the adamantoid cluster cage.

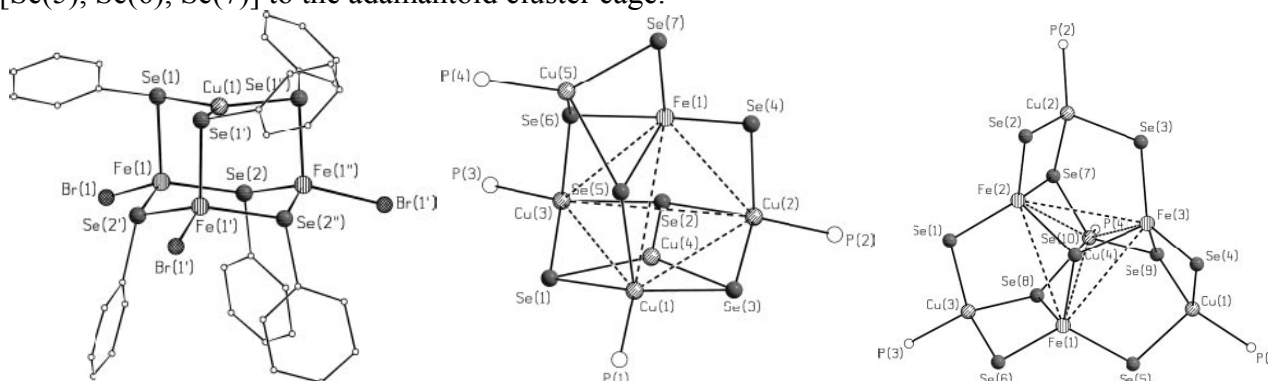
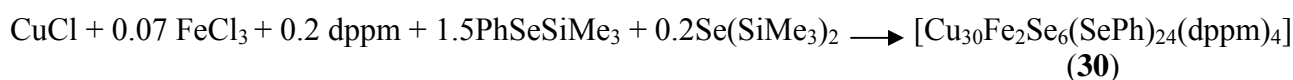


Figure 13 .Molecular structures of: *left*: cluster anion $[\text{CuFe}_3\text{Br}_3(\text{SePh})_6]^{2-}$ in **27**; *middle*: $[\text{Cu}_5\text{Fe}(\text{SePh})_7(\text{PPh}_3)_4]$ (**28**); *right*: $[\text{Cu}_4\text{Fe}_3(\text{SePh})_{10}(\text{PPh}_3)_4]$ (**29**); Phenyl groups omitted.

Similar to **27**, the structure of **29** contains a central CuFe_3 unit. Thus, three iron atoms define the vertices of the basal triangular plane, which is bridged by a $\mu_3\text{-SePh}^-$ ligand, while the apex of the pyramid is occupied by a CuPPh_3 unit. The other faces of the pyramid are capped by three distorted tetrahedral $\text{PPh}_3\text{Cu}(\text{SePh})_3$ units in such a way that six SePh^- ligands [$\text{Se}(1)\text{--Se}(6)$] adopt a μ_2 - and three [$\text{Se}(8)\text{--Se}(9)$] a μ_3 -bridging mode, which results in an overall distorted tetrahedral coordination of the metal atoms. All copper atoms are surrounded by two $\mu_2\text{-SePh}^-$ moieties, one $\mu_3\text{-SePh}^-$, and a terminal PPh_3 ligand. The iron atoms are four-coordinated by two $\mu_2\text{-SePh}^-$ and two $\mu_3\text{-SePh}^-$ ligands. Obviously, the core of the cluster complex comprises a pseudo-threefold axis running through $\text{Se}(10)$, $\text{Cu}(4)$, and $\text{P}(4)$; however, the organic ligands do not have this symmetry.

The reaction of CuCl and FeCl_3 with a mixture of $\text{Se}(\text{SiMe}_3)_2$ and PhSeSiMe_3 (Scheme 6) leads to the formation of $[\text{Cu}_{30}\text{Fe}_2\text{Se}_6(\text{SePh})_{24}(\text{dppm})_4]$ (**30**).



Scheme 6

Figure 14 shows the structure of compound **30**, consisting of 30 copper and two iron atoms.

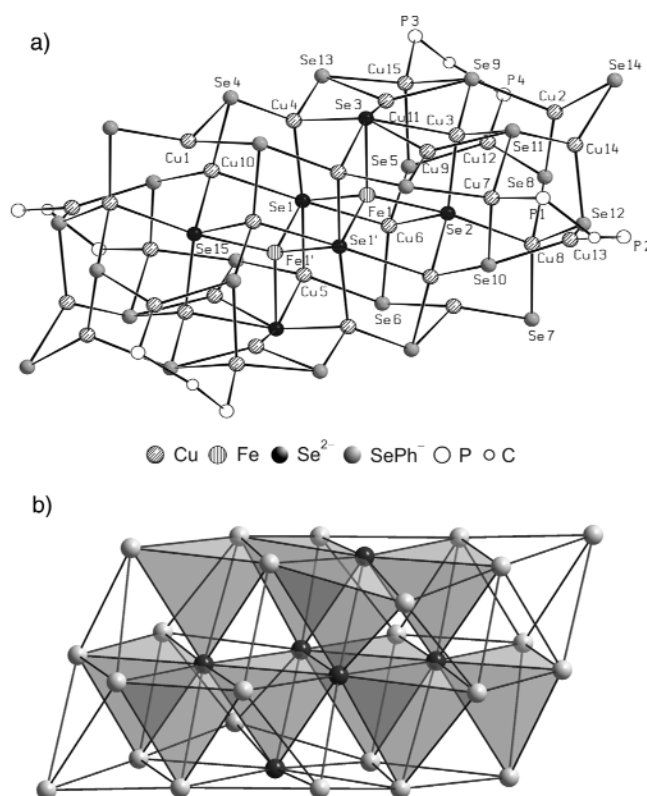


Figure 14. *top* molecular structure of $[\text{Cu}_{30}\text{Fe}_2\text{Se}_6(\text{SePh})_{24}(\text{dppm})_4]$ (**30**), (without C and H atoms, only the C atoms of the CH_2 group of the dppm ligands are drawn); *bottom*: Se sub-structure.

Assuming that the selenium atoms are charged 2- and that the SePh groups are charged 1-, 36 positive charges must be divided by the 32 metal atoms. This leads to three possible models:

- 1) Assuming that there is no Fe present in the cluster: 28 Cu^{1+} and 4 Cu^{2+}
- 2) Assuming Fe to be present: 28 Cu^{1+} and 4 Fe^{2+} , or
- 3) 30 Cu^{1+} and 2 Fe^{3+} .

Model 1 can be excluded because **30** is only formed in the presence of FeCl₃. The presence of two iron atoms as shown in Figure 14 could be verified by XANES measurements. In contrast to pure Cu-Se clusters the iron containing cluster **30** shows significantly different optical properties with a shift of the absorption to longer wavelengths. Using Mössbauer spectroscopy it was possible to show that the iron atoms are in the oxidation state 3+. This assumption is also verified by magnetic measurements showing a strong antiferromagnetic coupling between the iron atoms.

5 Silver Sulfide Clusters [18, 19]

There are a number of silver chalcogenide cluster complexes known. Examples of these compounds are listed in Table 3.

Ag-S cluster	Ag-Se cluster	Ag-Te cluster
[Ag ₂ (PSh) ₂ (dppe) ₃]	[Ag ₃₀ Se ₈ (Se <i>t</i> Bu) ₁₄ (P <i>n</i> Pr ₃) ₈]	[Ag ₅ (TePh) ₆ (Ph ₂ P(CH ₂) ₂ PPh ₃)(Ph ₂ P(CH ₂) ₂ pPh ₃)]
[Ag ₇ (PSh) ₇ (dppm) ₃]	[Ag ₉₀ Se ₃₈ (Se <i>t</i> Bu) ₁₄ (PEt ₃) ₂₂]	[Ag ₁₈ (Te(TePh) ₁₅ (Ph ₂ P(CH ₂) ₃ PPh ₂) ₃ Cl)]
[Ag ₂₂ Cl(SPh) ₁₀ (PhCO ₂) ₁₁ (dmf) ₃]	[Ag ₁₁₄ Se ₃₄ (SenBu) ₄₆ (P <i>t</i> Bu ₃) ₁₄]	[Ag ₃₈ Te ₁₃ (Te <i>t</i> Bu) ₁₂ (Ph ₂ P(CH ₂) ₂ PPh ₂) ₆]
[Ag ₇₀ S ₂₀ (SPh) ₂₈ (dppm) ₁₀](CF ₃ CO ₂) ₂	[Ag ₁₇₂ Se ₄₀ (SenBu) ₉₂ (Ph ₂ P(CH ₂) ₃ PPh ₂) ₄]	
[Ag ₈₈ S ₉₄ (P <i>n</i> Pr ₃) ₂₀]	[Ag ₁₂₄ Se ₅₇ (Se <i>t</i> P <i>t</i> Bu ₂) ₄ Cl ₆ (<i>t</i> Bu ₂ P(CH ₂) ₃ P <i>t</i> Bu ₂) ₁₂]	
[Ag ₂₆₂ S ₁₀₀ (S <i>t</i> Bu) ₆₂ (dppb) ₆]		
[Ag ₃₆₀ S ₁₃₅ (S <i>t</i> Bu) ₉₄]		

Table 3. Examples of known Ag-chalcogenide clusters [20]

All these compounds have been synthesized in Karlsruhe. During the last few years we focused our interest in the synthesis of nanoscaled Ag-S clusters. These compounds are formed in high yields by the reaction of silver halides in the presence of tertiary phosphanes and silylated derivatives of sulfur. To get very large clusters we found that the salts AgSR (R = org. group) are useful starting materials in reactions with S(SiMe₃)₂ and a tertiary phosphane.



Scheme 7. Synthesis of new Ag-S clusters **31** to **35**.

The formation of **31** to **35** is only possible in the presence of bidentate phosphane ligands, but only in **33** these ligands are found in the final product. Such compounds can be regarded as intermediates in the formation of bulk Ag₂S, in which phosphane and the SR-ligands have inhibited further growth of the cluster core towards crystalline Ag₂S. In most of these compounds there is a tendency to disorder structures. In this respect the molecules already possess to a large extent the properties of the Ag₂S bulk phase.

The structural determinations of these large clusters proved problematic. With nuclearities of up to 100 metal atoms, crystals generally diffract well to up high 2θ values (50–60° with MoKα); the atoms have low temperature factors, and no high residual electron density is observed within the clusters. However, this situation changes for larger clusters with nuclearities greater than around 120 metal atoms. For such clusters, the intensities of the reflections drop off rather sharply above 2θ ≈ 40°, and the structure refinement results in unsatisfactorily high R factors, with high residual electron density within the cluster molecule. Satisfactory R factors can only be obtained if this electron density can be modelled during the refinement. As this electron density generally lies close

to the heavy atoms, it can be difficult to interpret and thus complicates efforts to give precise estimates of the molecular formulae. These effects may result from a range of factors:

- 1) There is no perfect translational order in the lattice.
- 2) With the silver-chalcogenide clusters there is a tendency towards non-stoichiometry, as is seen for the binary phases. This behavior could be a consequence of the rather similar electronegativities of silver and the chalcogenides. There is no clear distinction between Ag^+ and E^{2-} (E=S, Se, Te), and the clusters behave rather like alloys.
- 3) The surface tension of the spherical molecules generates a Laplace pressure within the molecule, which can result in a disorder or even a phase transition.
- 4) Interactions between defects within the clusters can themselves lead to an increase in the defect concentration.

It is therefore no longer possible, in a strict sense, to obtain precise molecular formulae of these large clusters from their structure determinations. One can only think in terms of “idealized” formulae, resulting from the assumptions that non-bonded $\text{Ag}\cdots\text{Ag}$ distances are larger than 280 pm and that nonbonding $\text{S}\cdots\text{S}$ or $\text{S}\cdots\text{Se}$ distances are at least 410 pm. It is conceivable that different spatial arrangements of Ag^+ and chalcogenide ions can be accommodated below the ordered surface of the cluster. This possibility is supported by the observation that datasets measured from crystals obtained from different synthetic reactions can often not be refined with the same set of coordinates for the Ag, chalcogen, and carbon atoms, even though they have the same unit cells. Furthermore, one often observes a broad distribution of molecular ions in the mass spectrum. The structural determination of such large cluster molecules is thus pushing the currently available techniques to their limits, and it must be accepted that at present they may not always be able to give a satisfactory answer.

One can even describe the structures of **31** to **35** as nanoparticle with an ordered surface. Inside is a solid solution of Ag_2S . As a consequence about 10 % of the Ag and S atoms are disordered.

A crystal structure analysis shows that **31** crystallises in the space group $R\bar{3}c$ with six molecules per unit cell and 15 disordered toluene per formula unit. According to the structure analysis the formula of **31** is $[\text{Ag}_{123}\text{S}_{35}(\text{StBu})_{50}]$. In this case the cluster should have a charge of 3+. However a close inspection of the structure did not reveal the presence of anionic counterions. It is therefore assumed, that there is a nonstoichiometric Ag:S ratio as has been found in other metal chalcogenide clusters. This situation is not surprising, because this effect is also observed in solid Ag_2S .

From Figure 15 it can be seen, that the sulfur atoms of the *StBu* on the clustersurface act as μ_2 - or μ_3 -ligands. The S^{2-} ions show different bonding modes. S11 is a μ_4 -ligand, S10 and S12–S14 are bonded as μ_4 -ligands and S15 and S16 as μ_7 -ligands.

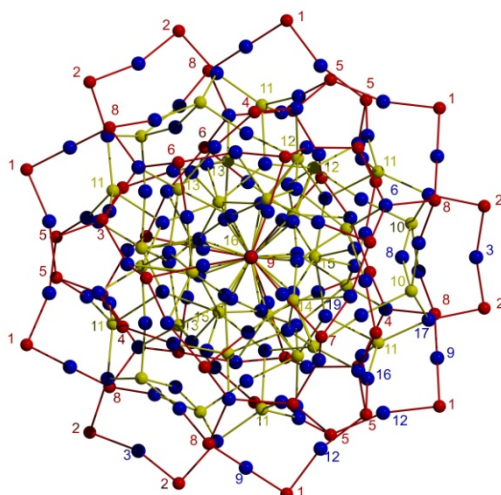


Figure 15. Molecular structure of **31** with *t*Bu groups omitted. For clarity the atoms are only numbered: blue: Ag^+ ; red: S atoms of the *St*Bu groups; yellow: S^{2-} atoms.

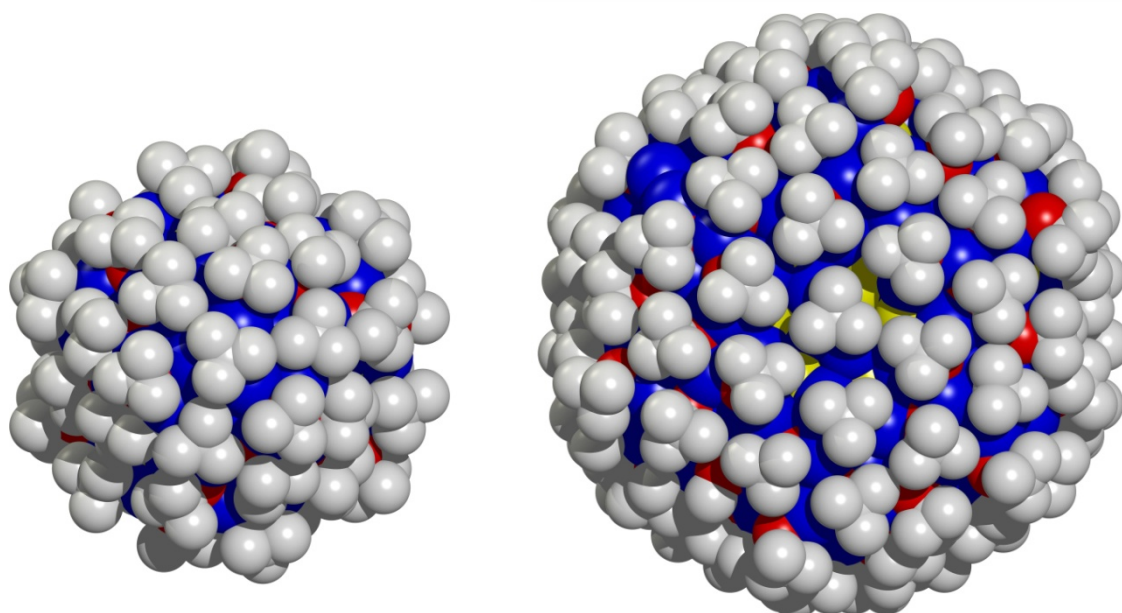


Figure 16. Space-filling models of **31** (*left*) and **32** (*right*) to the same scale. Gray: C; blue: Ag^+ ; red: S atoms of the *St*Bu groups; yellow: S^{2-} .

The space-filling model of **31** in Figure 16 (*left*) shows that the Ag-S-core, which has a maximum diameter of 1.7–2.0 nm, is completely shielded by the *t*Bu groups of the *St*Bu ligands in the oblate-spheroidal cluster. Further cluster growth is thus not possible. The maximum diameter of the molecule including the *t*Bu groups is 2.0–2.5 nm. Under different synthetic conditions we observed the formation for the metal-rich cluster **32**. Crystal-structure analysis shows that **32** crystallizes in the space group $C2/c$ with four molecules per unit cell. The cluster molecules form a quasi cubic close packing in the lattice, with the 12 disordered toluene molecules per formula unit situated in the holes. In Figure 16 (*right*) a space-filling diagram of **32** is shown. As in **31**, the cluster surface is covered exclusively by *t*Bu groups. The maximum total diameter of the molecule is 3.7 nm. The molecular shape is similar to an ellipsoid, which has a minor diameter of 2.6 nm. The dimensions of the Ag-S core are 3.2 and 2.2 nm. A precise description of the formula of **32** is, however, not possible from the structural analysis alone. The molecules are clearly not well ordered in the lattice.

We have measured 20 data sets from different crystals at different temperatures. None of these led to an improved interpretation of the structure. It is of note, however, that the outermost cluster layer of 96 AgStBu groups is ordered. The nearer the Ag and S atoms lie to the center of the cluster, the higher the degree of disorder. This situation is revealed in the higher temperature factors of the inner Ag and S layers. In this sense **32** is comparable with the structure of $[\text{Ag}_{262}\text{S}_{100}(\text{StBu})_{62}]$, although the degree of disorder is clearly higher in **32**. In both cases there is an ordered layer surrounding a solid solution of Ag_2S . Assuming that nonbonding Ag–Ag distances are greater than 2.80 Å, and bonding Ag–S interactions are in the range 2.40–2.90 Å, the formula $[\text{Ag}_{344}\text{S}_{124}(\text{StBu})_{96}]$ can be obtained. The elemental analysis of **32** is in excellent agreement with this formula. The experimental density of the crystal is also consistent with the density calculated from the X-ray crystal structure. The MALDI-TOF mass spectrum of **32** shows broad mass distribution with maxima at m/z 49446, 93104, 135586, 176572, and 216487 (Figure 17). At higher resolution, molecular ions with m/z 258028 and 298149 can be assigned. The molecular weight of **32** (49645 Da) is, allowing for the errors in the determination of the peak maxima, in good agreement with the signal at m/z 49446. Between the individual maxima a difference of approximately 41500 Da is found. This mass could be assigned to $[\text{Ag}_{344}\text{S}_{124}]^+$ (41046 Da), the molecule fragment of **32** from which all the StBu groups have been lost. The higher masses are likely to result from aggregates with unknown composition, which are formed from these molecular ions under the conditions of the MALDI-TOF experiment.

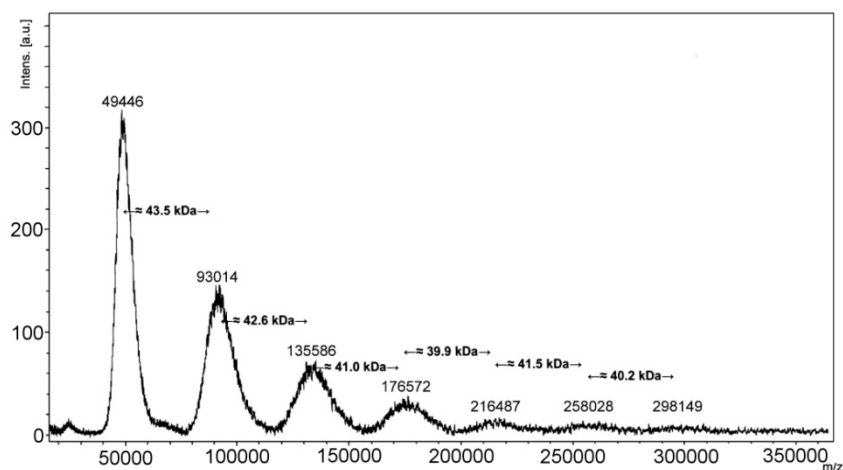


Figure 17. MALDI-TOF spectrum of **32**.

Additional evidence for the proposed formula of **32** is obtained through transmission electron microscopy (TEM) investigations of the reaction solutions from the synthesis of **32**. Such TEM images, shows particles with a monodisperse size distribution and a diameter of approximately 3 nm (Figure 18). This diameter corresponds to the size of the Ag–S-core in **32**. Further elucidation of the structure of the cluster is however not possible, since upon irradiation of the cluster for a long time the Ag–S cluster is converted into silver. Sometimes we even observed the formation of larger Ag particles. This is a result of a fusion of small Ag clusters to larger particle.

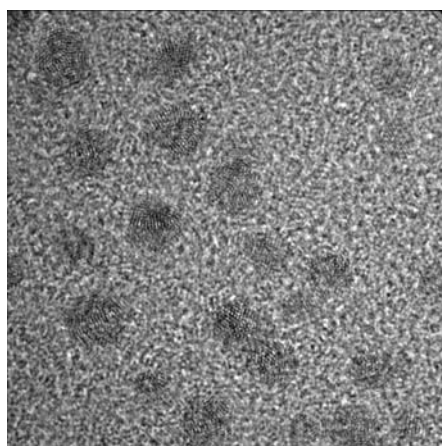


Figure 18. Electron microscope image of Ag clusters

This change is to be expected since Ag_2S decomposes at temperatures above 200 °C. Figure 19 illustrates the molecular structure from two directions, with the disorder omitted for clarity. The sulfur atoms of the *S**t*Bu groups act as μ 2- and μ 3-bridging ligands. The Ag–S distances are similar to those found in **31**. It is possible that the observed disorder is an intrinsic problem of nanoscopic Ag–S clusters. The surface tension of these particles gives rise to a Laplace pressure which in turn leads to a pressure within the particles, which is dependent upon particle radius. This pressure can result in disorder or a phase change. The transition of crystalline *a*- Ag_2S into the tetragonal high-pressure phase has been reported. Another explanation is that interactions between defects in the cluster can lead to a rise in the concentration of defects. This defect concentration is temperature dependent. To test this idea we have collected X-ray data sets over the temperature range 100–200 K. Measurement at higher temperatures is not possible because the crystals lose solvent and become amorphous. Over this temperature range, however, no increase in the disorder could be determined.

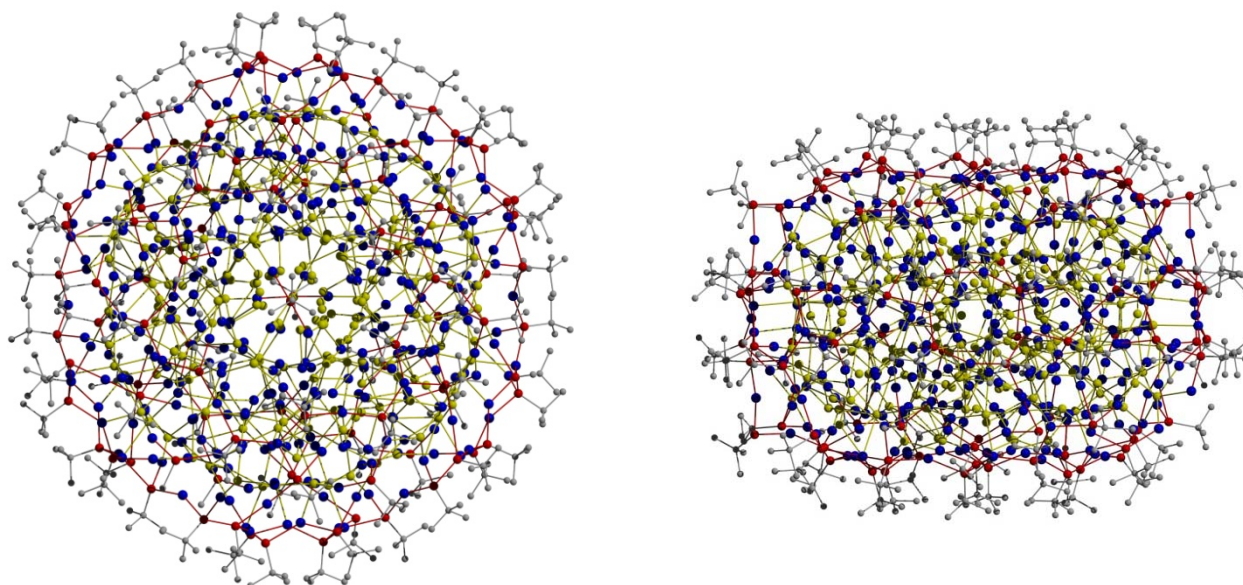


Figure 19. Molecular structure of **32** viewed from two directions. For clarity, the disorder is omitted. The right image is rotated by 90° relative to the left. Color code: blue: Ag^+ ; red: S atoms of the *S**t*Bu groups; yellow: S^{2-} .

In conclusion, **31** and **32** can be described as core-shell particles. In **31** the core is $\{(\text{Ag}_2\text{S})_{35}\text{Ag}_3\}^-$, and in **32** $\{(\text{AgS})_{124}\}$, the core in **31** is surrounded by a shell of 50 *S**t*Bu units and in **32** by 96 *S**t*Bu units. We believe that clusters that are metal-richer and have larger particle diameters can be

synthesized. These may, as a consequence of the lower Laplace pressure, have an ordered $\{(Ag_2S)_n\}$ core.

Meanwhile it is clear, that the ligands on the cluster surface are very important for the cluster structure. Just little changes of the size of the ligand and the reaction conditions yield new structures. In all cases we studied so far the presence of phosphanes is important. To synthesize **31** and **32** we used dppm (Bis(diphenylphosphanyl)methane). The same reaction of $AgStBu$ and $S(SiMe_3)_2$ in the presence of dppp (Bis(diphenylphosphanyl)propane) results in the formation of **33** (Scheme 7).

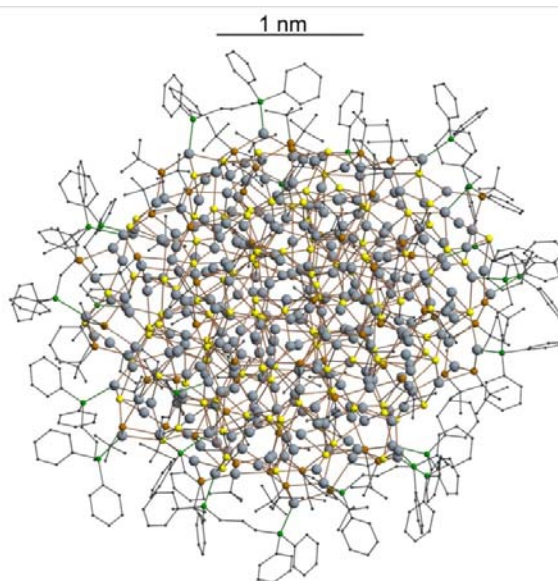


Figure 20. Structures of **33**, Ag gray, Se red, S in $StBu^-$ orange, S^{2-} yellow, C gray (small spheres), P green.

The molecular structure of **33** (fig. 44) consists of a $\{Ag_{260}S_{130}\}$ cluster core, to which 60 $AgStBu$ groups are attached; 24 Ag^+ ions are ligated by phosphorus atoms of the dppp ligands. The phosphane ligands together form a belt, which covers the equator of the spherical molecule. These P-coordinated Ag centers have either trigonal-planar (8) or tetrahedral (14) environments, and additional coordination from two or three S^{2-} ions, respectively. Only two Ag^+ ions have each one P and one S atom forming a quasi-linear coordination environment. All the other Ag^+ ions on the surface of the cluster have either distorted linear or trigonal-planar environments about the S atoms. Only those within the cluster are bonded to four S^{2-} atoms. As expected, the mean Ag-S distance increases with increasing coordination number. The ellipsoidal cluster core has a diameter of 2.4–2.9 nm; if the organic ligand shell is included, this value rises to an overall particle size of 3.3–3.9 nm. This result is in agreement with TEM images of **33**. The bidentate ligand dppp was employed in the synthesis of **33**, and it appears to have the appropriate steric requirements to coordinate to a cluster the size of **33**. If, however, dppbp is used, no product is observed. The formation of **34** and **35** is only possible in the presence of bidentate phosphanes. At present we do not know the reason for this. The structure of **34** (Figure 21), an oblate ellipsoidal shape, shows great similarities to that of $[Ag_{344}S_{124}(StBu)_{96}]$. However, by contrast, cluster **39** has StC_5H_{11} instead of $StBu$ groups as ligands on the surface, although this seems to result in only a small structural change. It is likely that all the 96 $\mu 2-$, $\mu 3-$, and $\mu 4-$ S atoms on the cluster surface belong to StC_5H_{11} groups, but only 84 of these 96 tC_5H_{11} groups could be located in the structure. However, allowing for this, we can arrive at an idealized formula $[Ag_{352}S_{128}(StC_5H_{11})_{96}]$.

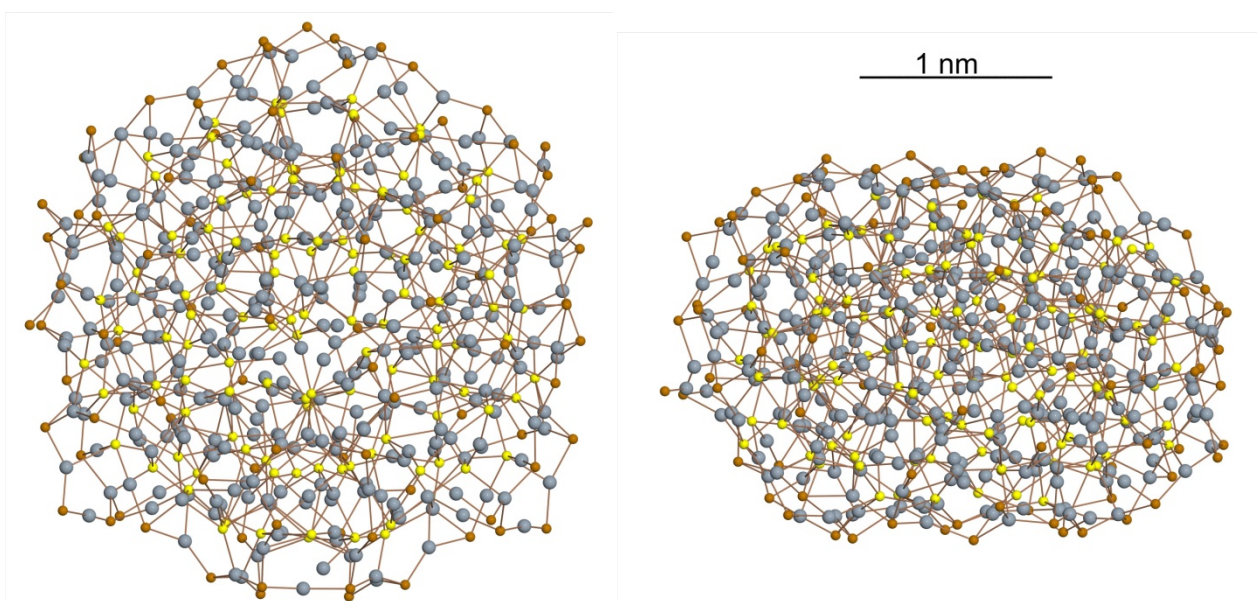


Figure 21. *left*: structure of **34** (C atoms of the C_5H_{11} groups omitted); *right*: structure of **34** rotated by 90° . Ag grey, S in $SC_5H_{11}^-$ orange, S^{2-} yellow.

It appears that **34** is only an intermediate product in the formation of the larger cluster in compound **35**. Under the reaction conditions described, **34** is only ever obtained in low yield. The principal product is always black hexagonal or rhombic crystals of **35**. The structure analysis shows that the hexagonal crystals crystallize in the trigonal space group $P3_221$ and the rhombic crystals in the monoclinic space group Cc . However, MALDI-TOF mass spectra indicate that the same compound is involved in both cases. In any case, we came up against substantial problems in solving and refining the crystal structures. Figure 22 shows the structure of **35** (with the tC_5H_{11} groups bonded to the surface S atoms omitted) viewed from two different directions. It proved to be very difficult to locate and refine many of the tC_5H_{11} groups, so in accordance with previous results the $\mu 2$ -, $\mu 3$ -, and $\mu 4$ -S atoms on the surface of the cluster were assumed to belong to StC_5H_{11} groups, giving a total of 114 StC_5H_{11} ligands. Of these 114 disordered groups, only 108 could be located.

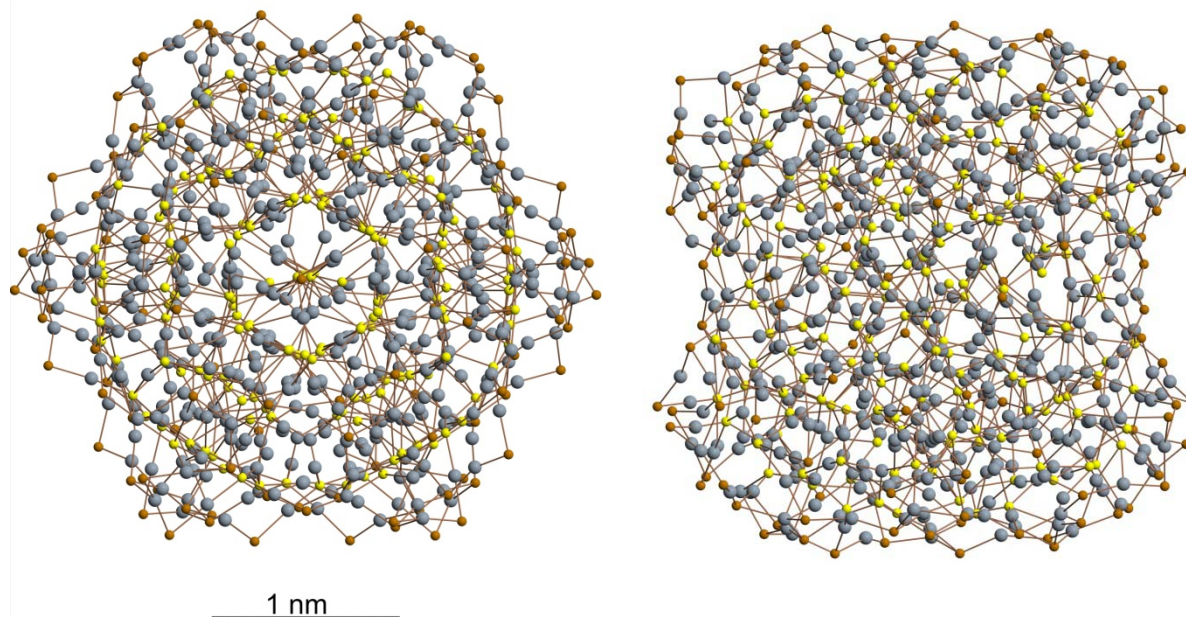


Figure 22. *left*: structure of **35** (C atoms of the C_5H_{11} groups omitted); *right*: structure of **35** rotated by 90° . Ag gray, S in $SC_5H_{11}^-$ orange, S^{2-} yellow.

The AgS core in **34** has the form of a flattened sphere of diameter 2.3 nm, or 2.5–3.5 nm if the C_5H_{11} groups are included. In **35**, the AgS cluster can be described as a narrow-waisted cylinder of dimensions 2.8–3.1 nm. If the tC_5H_{11} groups are included, the diameter increases to 3.3–3.6 nm. As for **34**, the Ag and S atoms within the cluster are substantially disordered, and the formula can only be idealized as $[Ag_{490}S_{188}(StC_5H_{11})_{114}]$, which would have a formula weight of 70650 Da. In fact, MALDI-TOF measurements from a number of crystals indicate that the maxima in the molecular weight vary between 65846 and 68032 Da, even though their unit cell geometries do not vary significantly. It is also clear that the distribution of molecular weights within a spectrum is very broad (61000–74000 Da). This result is in agreement of the findings of other authors who have used MALDI-TOF methods to characterize nanoparticles. From these previous results from related nanoclusters, it is clear that organic or SR groups are very easily lost by fragmentation under the conditions of MALDI-TOF experiments. For this reason, interpretation of such mass spectra is not straightforward; however, it is nonetheless striking that a broad distribution of high masses appears in the MALDI-TOF spectrum of **35** (Figure 23). In addition to the maximum at 68033 Da, there are also maxima at 128331, 185171, 242477, 300231, 366273, and 456879 Da.

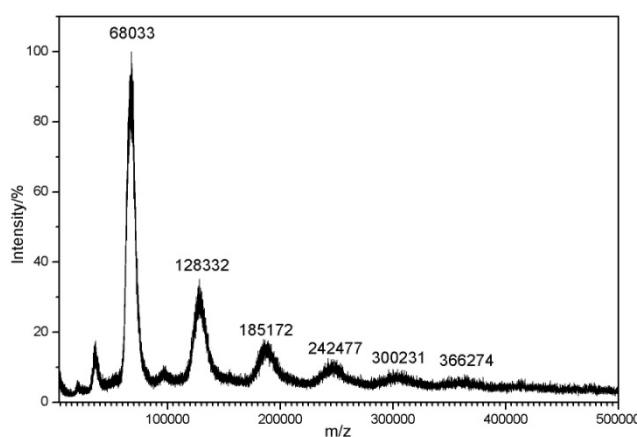
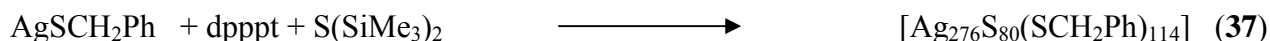
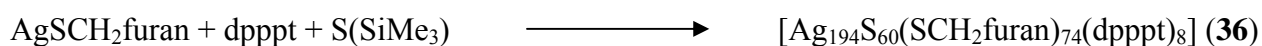


Figure 23. MALDI-TOF spectrum of **35**.

This distribution evidently results from cluster aggregation, which can occur in the plasma created by laser excitation. The difference in mass between the maxima is around 57500 Da, which is very close to the mass of the fragment that would result from the loss of all the StC_5H_{11} groups from **35** ($\{Ag_{490}S_{188}\}$: 58880 Da). From samples prepared under different experimental conditions one can also observe a very narrow distribution of masses at 59200 Da. It is possible that a variable number of Ag_2S units could be arranged under the shell of the 114 $AgStC_5H_{11}$ groups. For this reason, a precise molecular formula cannot be obtained from the structural analyses; instead, in agreement with the MALDI-TOF results, we must be content with a range of compositions. We then arrive at $[Ag_{(474-490)}S_{(180-188)}(StC_5H_{11})_{114}]$ as the best formulation. In this case, 490 Ag atoms correspond to full occupancy of all sites in the structure, whereas the lower number is the formula obtained from the lowest observed molecular mass. In this respect, these compounds behave in a similar manner to binary Ag_2S , for which a range of compositions is also observed. The geometries and bond lengths for the Ag and S atoms of the $StC_5H_{11}^-$ and S^{2-} ligands are similar to those in **33** and **34**, but given the degree of disorder a more detailed discussion is not advisable.

As already mentioned above both the organic groups bound to the sulfur atoms and the phosphanes have a big influence on the formed cluster structure. This can be demonstrated by using different reactants as shown in Scheme 8.



Scheme 8. Syntheses of 36-39. dpppt = Bis(diphenylphosphino)pentan

Figure 24 shows the structure of $[\text{Ag}_{194}\text{S}_{60}(\text{SCH}_2\text{furan})_{74}(\text{dpppt})_8]$ (**36**).

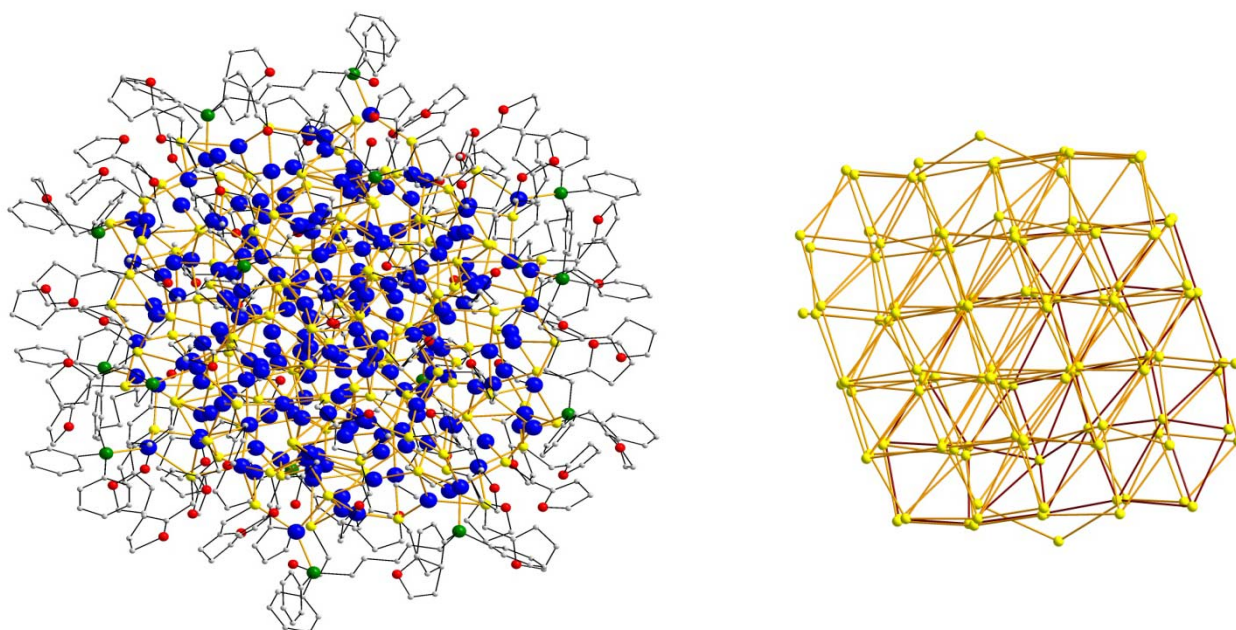


Figure 24. left: molecular structure of $[\text{Ag}_{194}\text{S}_{60}(\text{SCH}_2\text{Furan})_{74}(\text{dpppt})_8]$ (36**) right: sulfur sub-structure in **36**; Ag: blue; S: yellow; P: green; O: red.**

Figure 25 shows the molecular structure of **37** as ball and stick (left) and as space-filling model. For synthesizing the compounds **36** and **37** in both cases $\text{S}(\text{SiMe}_3)_2$ and the same phosphane (dpppt) but different silver thiolates were used. Obviously the small differences in the sterical demands of the thiolate substituents are the reasons for the formation of different cluster cores. Without any doubt the reactions leading to the final cluster are very complicated. It can be assumed that in a first step polynuclear silver thiolate phosphane complexes are formed. During the formation process these initial complexes react with $\text{S}(\text{SiMe}_3)_2$ yielding the final large clusters.

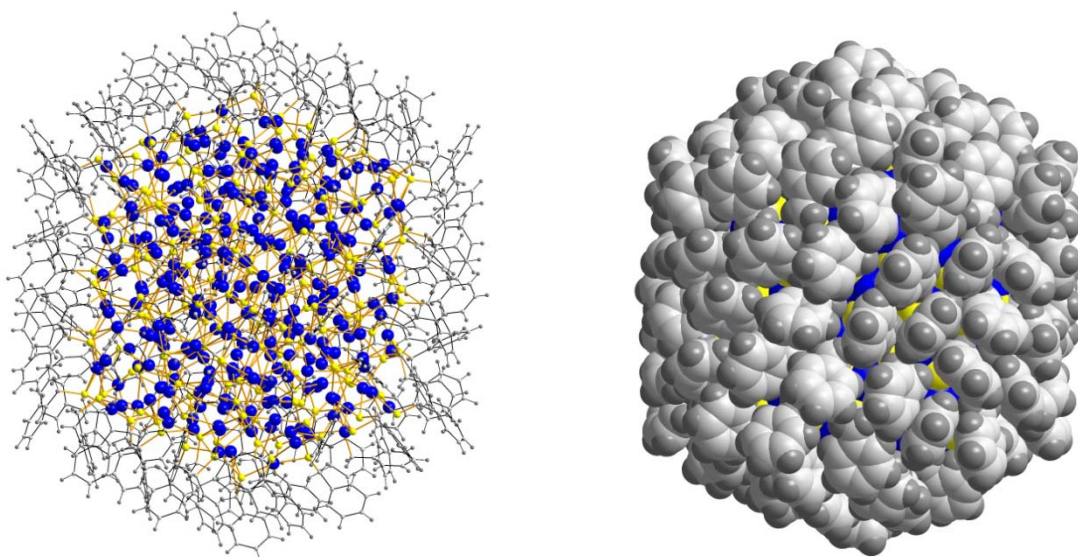


Figure 25. *left*: molecular structure of $[\text{Ag}_{276}\text{S}_{80}(\text{SCH}_2\text{Ph})_{114}]$ (28); *right*: space-filling model of 28 in the same orientation.

In the presence of a very bulky phosphane ligand ($\text{Ph}_2\text{PCH}_2\text{C}_6\text{H}_4\text{-C}_6\text{H}_4\text{CH}_2\text{PPh}_2$) the reaction of $\text{AgStC}_5\text{H}_{11}$ with $\text{S}(\text{SiMe}_3)_2$ leads to a mixture of the two different clusters $[\text{Ag}_{156}\text{S}_{60}(\text{StC}_5\text{H}_{11})_{36}]$ (38) and $[\text{Ag}_{360}\text{S}_{130}(\text{StC}_5\text{H}_{11})_{100}]$ (39). The Figure 26 and Figure 27 show the molecular structures of these compounds.

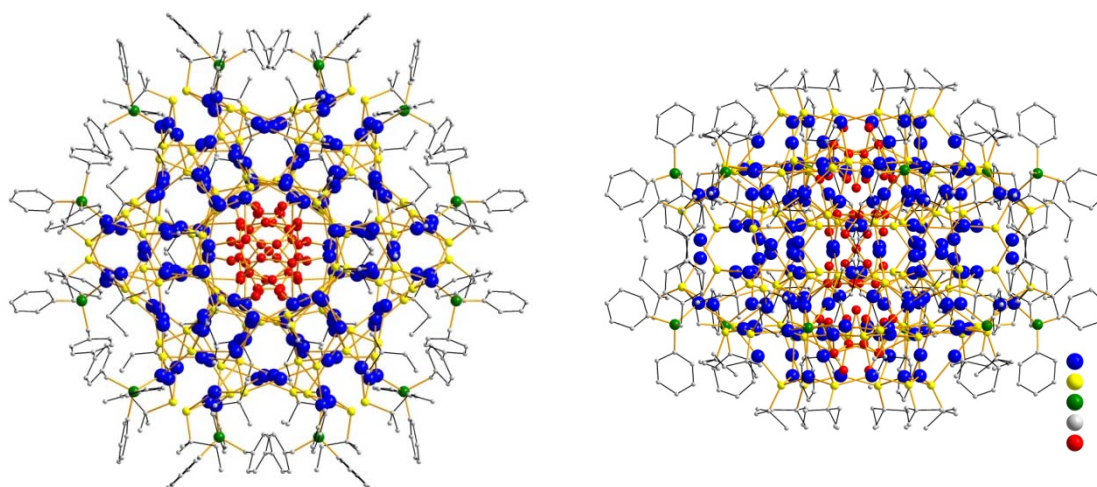


Figure 26. *links*: Molecular structure of $[\text{Ag}_{156}\text{S}_{60}(\text{StC}_5\text{H}_{11})_{36}]$ (38); *right*: structure rotated by 90° . Ag: blue; S: yellow, disordered Ag and S positions: red.

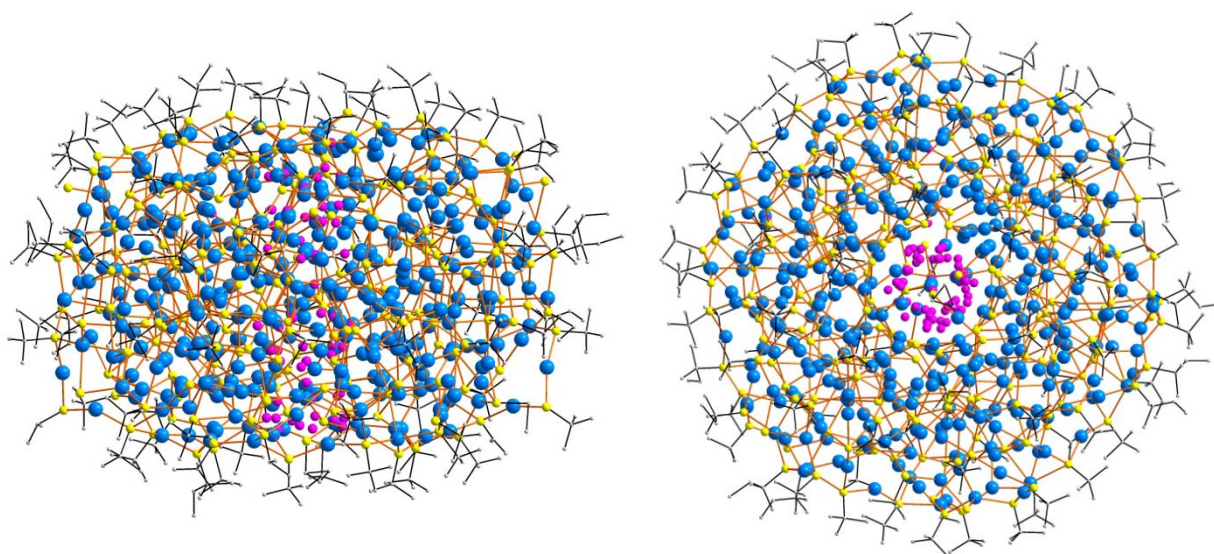


Figure 27. links: Molecular structure of $[\text{Ag}_{360}\text{S}_{130}(\text{StC}_5\text{H}_{11})_{100}]$ (**39**), *right:* structure rotated by 90° . Ag: blue; S: yellow, disordered Ag and S positions: red.

During the structural refinement of **38** 156 silver and 96 sulfur atoms could be located. After adding the carbon atoms of the ligand shell the R1 factor of 0.13 is found. Figure 26 shows that there is a cylindric area inside the cluster where high electron density remains. Some of these positions are only 120 pm away from the silver positions. The volume of the cylinder is aprox. 300 \AA^3 being space for six Ag_2S units which are statistcly dissorderd over the red positions in Figure 26.

Remarkably the same structural situation is found for **39** (Figure 27) again. As in **38** there is a dissorderd cylindrical area of approx. 300 \AA^3 in the centre the cluster. Maybe **38** acts as an intermediat during the formation of **39**. The structure of $[\text{Ag}_{360}\text{S}_{130}(\text{StC}_5\text{H}_{11})_{100}]$ (**39**) is very similar to the structure of $[\text{Ag}_{352}\text{S}_{128}(\text{StC}_5\text{H}_{11})_{96}]$ (**34**) which has been described above (Figure 21).

Assuming that in both cases the dissorderd area is filled with six Ag_2S units the two clusters can be formulated as $[\text{Ag}_{168}\text{S}_{66}(\text{StC}_5\text{H}_{11})_{36}]$ for **38** and $[\text{Ag}_{372}\text{S}_{136}(\text{StC}_5\text{H}_{11})_{100}]$ for **39**.

In conclusion, we must emphasize that the structures we have obtained for these large nanoclusters are by no means a perfect solution to the problem, but this is perhaps to be expected, as we are at the very edge of molecular chemistry.

6 Functionalized Silver-Chalkogen Clusters [21]

We also tried to synthesize Ag-S clusters with functionalised ligands on the surface. For example AgPhCO_2 , dppm, $\text{S}(\text{SiMe}_3)_2$ and $\text{Me}_2\text{N}-\text{C}_6\text{H}_4\text{SSiMe}_3$ yields to formation of $[\text{Ag}_{63}\text{S}_{13}(\text{SC}_6\text{H}_4\text{NMe}_2)_{39}(\text{dppm})_5]$ (**40**). In a similar reaction of AgPhCO_2 , PPh_3 , $\text{Se}(\text{SiMe}_3)_2$ and $\text{Me}_2\text{N}-\text{C}_6\text{H}_4-\text{SSiMe}_3$ we could isolate $[\text{Ag}_{76}\text{Se}_{13}(\text{SC}_6\text{H}_4\text{NMe}_2)_{50}(\text{PPh}_3)_{6.5}]$ (**41**) and $[\text{Ag}_{88}\text{Se}_{12}(\text{SC}_6\text{H}_4\text{NMe}_2)_{63}(\text{PPh}_3)_6]$ (**42**).

40–42 are built up in a shell-like manner. In the inner silver chalcogenide cores, the silver ions have linear, trigonal planar or tetrahedral coordination geometries. The cores are surrounded by organic shells consisting of phosphane ligands coordinated to silver ions and dimethylanilino groups bonded to sulfur atoms. **41** and **42** can be described as core–shell particles with silver selenide cores surrounded by silver sulfide shells.

The inner part of **40** (Figure 28, *top*) the cluster consists of 13 sulfur atoms (S40–S52) that do not bear any organic substituents and, therefore, have a charge of -2. This S_{13} core (orange in Figure 28, *top*) can be described as part of a double hexagonal close-packed (ABAC) lattice, with three sulfur

atoms (S40–S42) representing an A layer, six sulfur atoms (S43–S48) a B layer, three sulfur atoms (S49–S51) another A layer, and atom S52 a C layer. The core is surrounded by a shell of 39 sulfur atoms (yellow in Figure 28, top), each of which is bonded to a dimethylanilino group and has a charge of -1. However, these sulfur atoms are not arranged in close-packed layers. For charge balance, 65 silver ions are incorporated into the sulfur substructure. In the X-ray structure analysis, 60 of these ions were unambiguously located; the five remaining silver ions are disordered over 10 positions (Ag61–Ag70). The metal ions in the b-modification of Ag₂S are also severely disordered, resulting in a significant ionic conductivity. The inorganic part of cluster **40** consisting of silver and sulfide ions has a diameter of approximately 1.7 nm; if the organic shell of dimethylanilino groups and dppm ligands is also taken into account, the total particle size is approximately 2.8 nm.

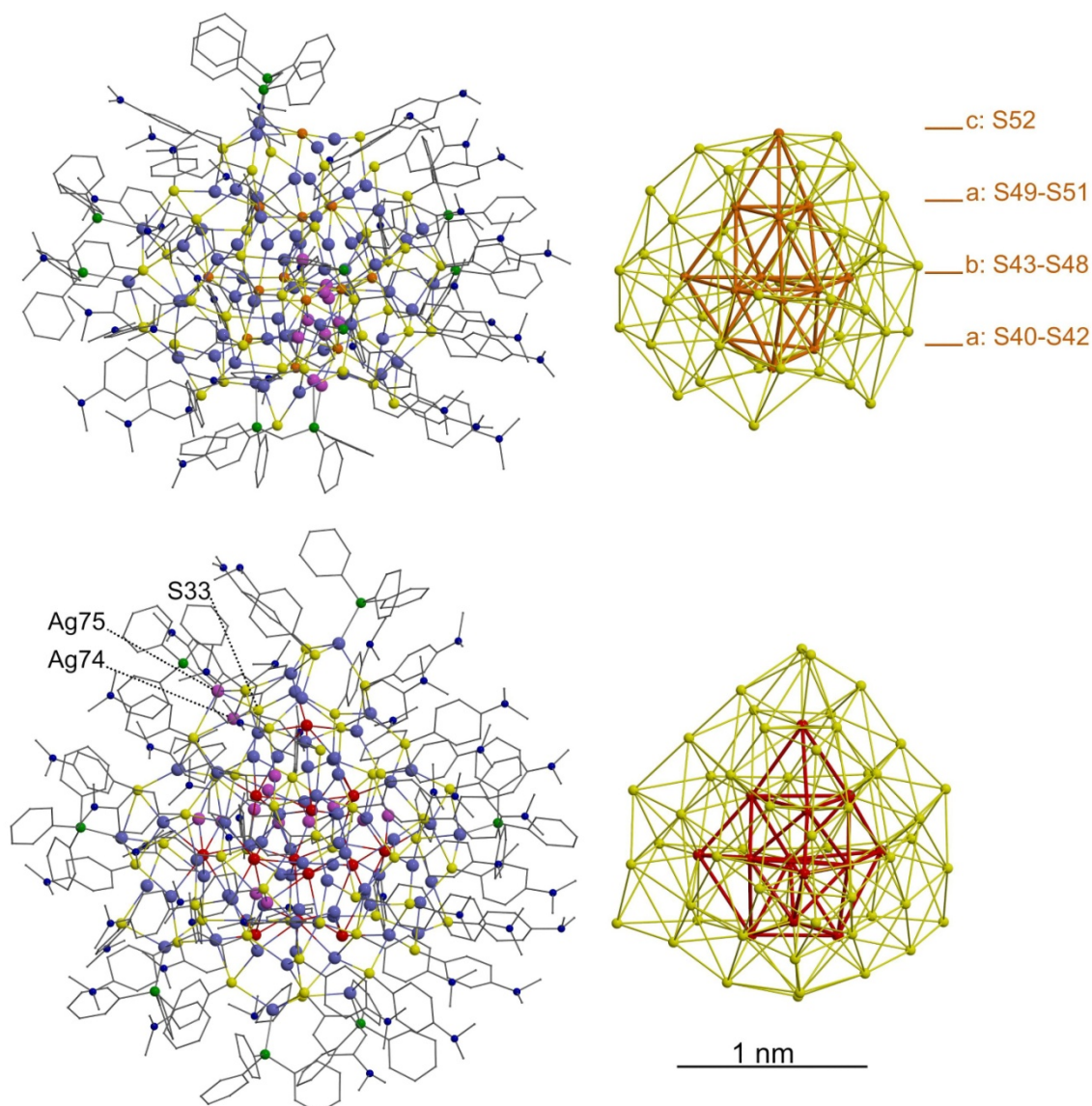


Figure 28. : Structures of clusters **40** (top) and **41** (bottom): the molecular structures (left) and the chalcogen substructures (right). Ag blue (disordered Ag violet), Se red, S²⁻ orange, SR yellow, P green, N small darkblue, C gray. The lines connecting the chalcogen atoms in the substructures are for visualization and do not represent bonds. The ABAC layers of the double hexagonal close-packed S²⁻ core of **41** are indicated (left).

Close examination of the structure of **41** (Figure 28, bottom) shows that **41** is a mixture of two different cluster compounds, one with the composition [Ag₇₆Se₁₃(SC₆H₄NMe₂)₅₀(PPh₃)₇] and the other with the composition [Ag₇₆Se₁₃(SC₆H₄NMe₂)₅₀(PPh₃)₆]. The structures of both clusters are identical, with the exception that the dimethylanilino group bonded to S33 has a different

orientation in each. Thus, in the first cluster, Ag75 bears a PPh₃ ligand, but in the second cluster this silver atom occupies position Ag74, which bears no PPh₃ ligand, in the inner part of the cluster. As a result, **41** has 6.5 PPh₃ ligands on average. Apparently, this small difference does not influence the arrangement of the two clusters in the crystal lattice. No indications of an ordered superstructure were observed; evidently, **41** is a cocrystal of two very similar clusters, which are randomly arranged in the lattice. The core of **41** consists of 13 selenium atoms (red in Figure 28, *bottom*), which are arranged in the same way as the S²⁻ ions in **40**. In **41**, the core is completely surrounded by the 50 sulfur atoms of the SC₆H₄NMe₂ groups. The selenide core of **41** has a diameter of nearly 1.1 nm; if the sulfide shell is also considered, the inorganic part of the cluster has a size of 1.9 nm. With the organic shell, **41** has a particle size of approximately 3.1 nm.

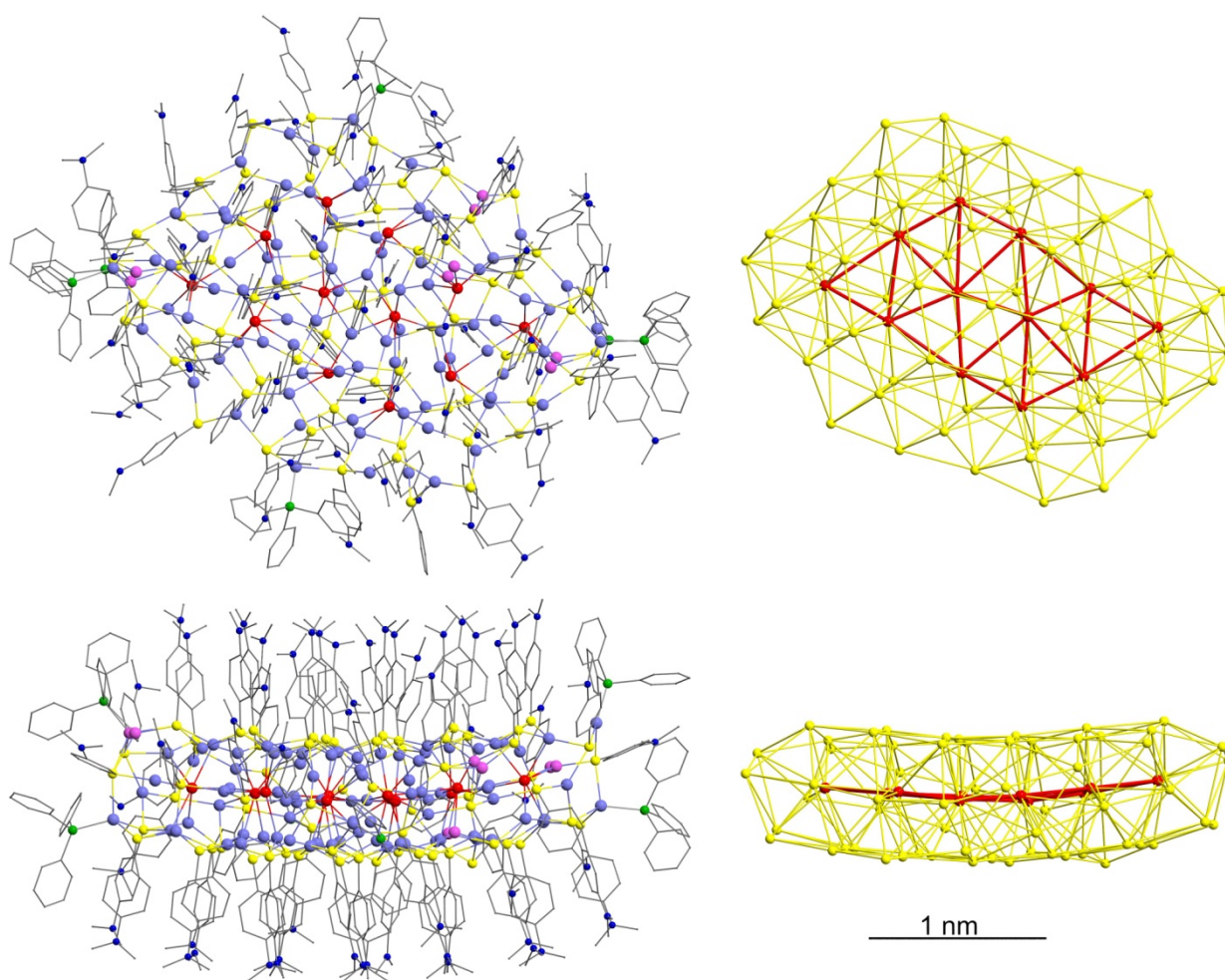


Figure 29. Structure of **42**: the molecular structure (left) and the chalcogen substructure (right) in two perpendicular projections (top and bottom). Ag blue (disordered Ag violet), Se red, S yellow, P green, N small darkblue, C gray. The lines connecting the chalcogen atoms in the substructures are for visualization and do not represent bonds.

In contrast to the nearly spherical clusters **40** and **41**, cluster **42** (Figure 29), which contains 88 silver atoms, has a layered structure. The 12 selenium atoms of the core (red in Figure 29) form a 3 x 4 hexagonal layer, which however, is not planar, but slightly bent. The core is completely surrounded by a shell consisting of 63 sulfur atoms; the atoms above and below the selenium layer are also arranged in a hexagonal pattern. The resulting charge for the chalcogenide substructure is -87. According to the X-ray structure analysis, there are 88 silver atoms in cluster **42**, one more than

is necessary for charge balance. Of these, 82 silver atoms occupy holes in the chalcogenide core and have linear, trigonal planar or tetrahedral coordination geometries. Only the six silver atoms bearing phosphane ligands are located outside of the sulfur shell; one is coordinated by two sulfur atoms and one phosphorous atom in a trigonal planar geometry, and the other five are bonded to three sulfur atoms and one phosphorous atom. In **42**, some silver atoms are again disordered. As no counterions were detected, one of the 88 silver atoms must be formally uncharged. However, no such atom could be identified on the basis of its coordination environment; rather, it is assumed that the +87 charge is equally distributed over the 88 silver atoms. This phenomenon is typical for the modifications of silver sulfide, which exhibit a certain phase width (Ag_{2+x}S). The plate-like silver chalcogenide core of **42** has dimensions of $0.5 \times 1.8 \times 2.2 \text{ nm}^3$. With its organic shell, the size of the whole cluster **42** is $2.0 \times 3.0 \times 3.3 \text{ nm}^3$.

In future we would like to investigate conductivity of single cluster molecules. In a first step functionalized cluster must be deposited onto a metal surface (or between electrodes). To get such model compounds we investigated reactions of silver benzoate with bis(diphenylphosphino)pentan (dpppt) and Me_3SiS -thiophe. Beside of very small black crystals which could not be characterized yet yellow crystals of compound $[\text{Ag}_{34}\text{S}_9(\text{S-thiophen})_{16}(\text{dpppt})_6]$ (**43**) could be isolated. As shown in Figure 30 the 16 sulfur atoms of the thiophen ligands are located at the surface of the ligand shell. At least a part of them should be able to act as anchors to a metal surface (see Figure 30, right).

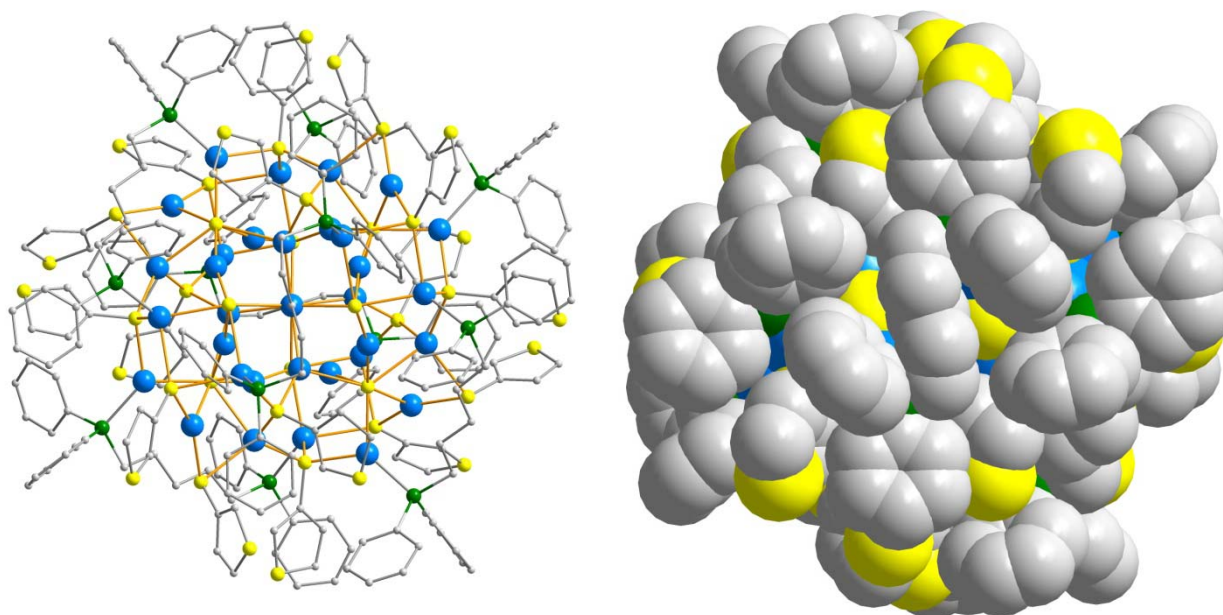


Figure 30. *left:* Molecular structure of $[\text{Ag}_{34}\text{S}_9(\text{S-thiophen})_{16}(\text{dpppt})_6]$ (**43**) (without H atoms). *right:* Space-filling model of **41**. Ag: blue; P: green; S: yellow.

Finally the synthetic concept described above can be used to synthesize other core shell particles consisting of an inner silver chalcogenide core surrounded by a silver chalcogenolate shell. Examples of these kind of clusters could have the compositions $[(\text{Ag}_2\text{Te})_m(\text{AgSR})_n]$, $[(\text{Ag}_2\text{S})_m(\text{AgSeR})_n]$ or $[(\text{Ag}_2\text{Te})_m(\text{AgSeR})_n]$.

We could already synthesize a series of such substances. One example is shown in the reaction in Scheme 9.



Scheme 9

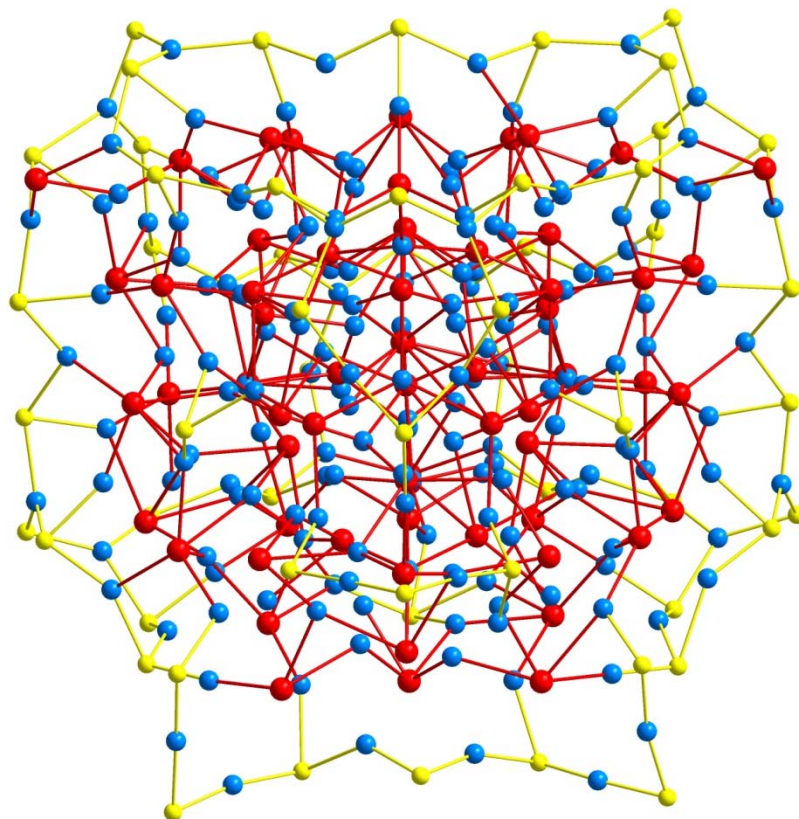


Figure 31. Molecular structure of the core of $[Ag_{182}Te_{63}(SC_6H_{13})_{56}]$ (**44**); Ag: blue, Te: red; S of SC_6H_{13} : yellow; C and H atoms omitted for clarity.

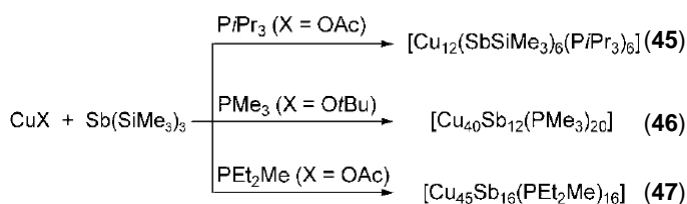
The structure of **44** (Figure 31) can be described as a $(Ag_2Te)_{63}$ core surrounded by a shell of $(AgSC_6H_{13})_{56}$.

7 Molecular alloy clusters [22, 23]

Recently we have started to study the synthesis and structural analysis of copper complexes containing heavier elements of Group 15. Despite the extensive amount of work that has been carried out in the area of transition-metal complexes of heavier Group 15 elements, there are only a few accounts of antimony- or bismuth-containing copper complexes. Most of these complexes are adducts of copper(I) salts with tertiary stibanes or bismuthines ER_3 ($E=Sb, Bi$; $R=aryl$ or $alkyl$) as terminal ligands. The first copper(I) antimonide complex $[\{Mes_2SbCu(PMe_3)_2\}_2]$ ($Mes=2,4,6$ -trimethylphenyl) was prepared by the metathesis reaction of Mes_2SbLi with $CuCl$. Our approach to the syntheses of copper(I) antimonides reported herein involves the reaction of $Sb(SiMe_3)_3$ with copper(I) salts in the presence of tertiary phosphines (see scheme 9). By this approach we have already synthesized the copper–antimony clusters $[Cu_{10}(Sb_3)_2(SbSiMe_3)^2(dppm)_6]$, $[Cu_{17}Sb_8(dppm)_7]$, and $[Cu_{20}Sb_{10}(PCy_3)_8]$ ($dppm = 1,2$ -bis-(diphenylphosphino)methane, $Cy=cyclohexyl$).^[24] The different ratio of Cu:Sb present in complexes **46** and **47** suggests copper atoms in the oxidation states 0, +I, or +II. UV/Vis studies and magnetic measurements on these type of compounds, however, did not confirm the presence of metal centers in various oxidation states and instead showed that these compounds are best described as phosphine-stabilized molecular copper–antimony alloys. On our way towards the selective synthesis of molecular alloys and the

correlation of their properties with those of CuSb phases which have similar Cu:Sb ratios, we report herein the structure of an intermediate copper–antimony cluster and the two largest molecular CuSb alloys belonging to this class of compounds [25]. The structures of the complexes were established by X-ray crystallography and the results assessed with structures obtained from DFT studies.

The reaction of CuOAc with Sb(SiMe₃)₃ in the presence of P*i*Pr₃ produced [Cu₁₂(SbSiMe₃)₆(P*i*Pr₃)₆] (**45**, Scheme 10). In the solid state **45** consists of a distorted centrosymmetric octahedral arrangement of six {SbSiMe₃} units. The copper atoms Cu(2,3,6) and their symmetry equivalents are each coordinated by one phosphorus atom of a P*i*Pr₃ ligand and two antimony atoms from an edge of the distorted Sb₆ octahedron (figure 57a).



Scheme 10. Synthesis of Cu–Sb clusters 45-47 (X=OtBu, OAc).

The remaining copper atoms Cu(1,4,5) and their symmetry equivalents are located on the faces of the Sb₆ octahedron and are coordinated by three Sb atoms. All the copper atoms have distorted trigonal planar coordination environments. A remarkable feature of **50** is that trimethylsilyl groups are still present despite the stoichiometric supply of starting materials (CuOAc:Sb(SiMe₃)₃=3:1). An explanation for this observation could be the presence of bulky *i*Pr₃P ligands which prevent **50** from further reactions with CuOAc. Compound **45** can be described as a “classical” Cu–Sb complex where charges can formally be assigned to give twelve Cu⁺ centres and six [SbSiMe₃]²⁻ ligands. Inspired by the structural diversity of copper clusters bridged by Group 16 elements, the reaction conditions (R groups of tertiary phosphines, anions of the CuI salts, and solvents), were modified. The reactions of PMe₃ with one equivalent of CuOtBu and then with Sb(SiMe₃)₃ produced black crystals of the copper–antimony clusters [Cu₄₀Sb₁₂(PMe₃)₂₀] (**47**) (Figure 32) and a complex which has the approximate composition [Cu₄₀Sb₂₁(PMe₃)₁₆] (**47a**). Crystals of **47** and **47a** can be separated manually under perfluoroether oil but decompose once placed under vacuum as a result of the loss of lattice-bound solvent.

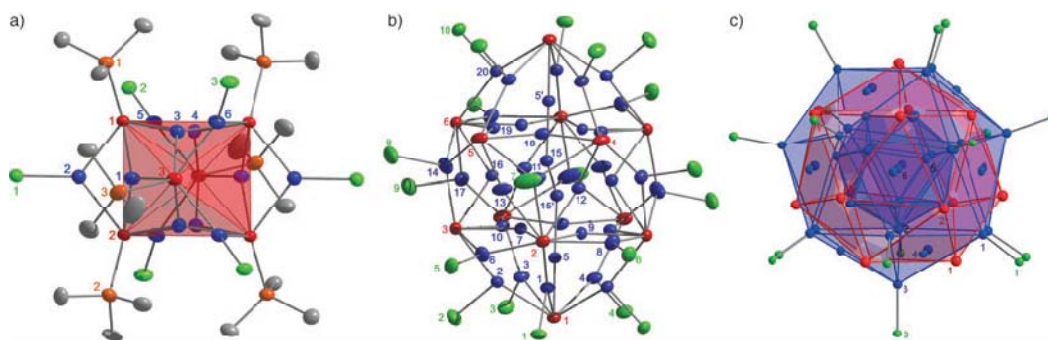


Figure 32. : a) Molecular structure of **45** (*i*Pr groups omitted); b) Molecular structure of **46** (Methyl groups omitted); c) Polyhedral representation of **47** (C and H atoms omitted). Color code: Sb red, Cu blue, P green C grey, Si orange.

Sb₁₂ unit. The copper atoms not coordinated by PMe₃ ligands are located inside the cluster. They bridge edges of the icosahedron and the atoms Cu(5), Cu(15), and their symmetry equivalents form a Cu₄ chain inside the cluster. The Cu⋯Cu distance of 2.316(2) Å between Cu(15) and Cu(15') is to our knowledge the shortest Cu–Cu distance observed to date in a molecular complex. The Sb-

46 consists of a distorted Sb_{12} icosahedron (nonbonding $\text{Sb}\cdots\text{Sb}$ distances ca. 5 Å). The twenty copper atoms located on the cluster surface are all coordinated to phosphorus atoms of PMe_3 ligands and bridge the edges or cap Sb_3 faces of the icosahedral Cu bond lengths in **46** (2.453(1)–3.162(2) Å) are characteristic for Cu–Sb complexes. Further experiments to elucidate the electronic structure and in particular the oxidation-state of the copper atoms involved were hindered by the unselective formation of **46** which makes it impossible to prepare larger amounts of pure **46** as it cannot be separated from the byproducts. Since the composition of **46** is non-stoichiometric with four excess electrons, density functional theory (DFT) calculations were carried out to investigate its electronic structure. The results show typical semiconductor features: the occupied valence band and the empty conduction band are separated by a band gap of about 1.5 eV, whereas orbital energies within these bands differ by typically 0.1 eV. A similar situation was observed in clusters of the composition $[\text{Cu}_{26}\text{Te}_{12}(\text{PEt}_2\text{Ph})_{12}]$, $[\text{Cu}_{32}\text{As}_{10}(\text{dppm})_8]$. In agreement with the small difference in electronegativities of Cu and Sb (Pauling scale: Cu 1.6, Sb 1.9), a valence band composed of 5p(Sb) and (4s)Cu orbitals is formed, which accommodates the four excess electrons. An “ionic” model of **46** which could consist of Cu^+ and Sb^{3-} ions and Cu^0 is inappropriate. A structural model of **46a** was also investigated using DFT methods and the results showed that the solution we obtained in the space group $F23$ was wrong. The DFT analysis was necessary because highly symmetric structures of large Cu–Sb clusters can sometimes not be determined reliably by X-ray crystallographic methods alone. This is due to the intrinsic problem that a crystal structure represents the arrangement of atoms averaged over a lot of molecules. For large clusters containing more than 60 metal atoms this means that metal atom positions in different cluster molecules can sometimes be occupied by Cu or Sb atoms. To gain further insight into this problem we have performed similar reactions of CuOAc and $\text{Sb}(\text{SiMe}_3)_3$ in the presence of phosphines and the reaction with PEt_2Me gave rise to another cluster containing the same number of metal atoms as **46a**. Black crystals were obtained from this reaction in addition to an amorphous black precipitate.

The X-ray analyses has shown that the structure can be solved in the cubic space group $F\bar{4}3m$. The cluster has the composition $[\text{Cu}_{45}\text{Sb}_{16}(\text{PEt}_2\text{Me})_{16}]$ (**47**) and consists of two metal shells (see figure 57c). The atom Cu(6) is in the center of **47** and is surrounded by a regular arrangement of 16 Cu atoms forming a slightly distorted Frank-Kasper polyhedron ($\text{Cu}(6)\cdots\text{Cu}$ 2.629(2) and 2.771(1) Å). Sixteen Cu atoms of the outer shell have a tetrahedral coordination environment and each one is bonded to a P atom of a PEt_2Me ligand and three Sb atoms. These Cu atoms and the outer Sb atoms are located on the corners of another Frank-Kasper polyhedron (with nonbonding $\text{Cu}\cdots\text{Cu}$ distances of ca. 4.1–4.9 Å; $\text{Sb}\cdots\text{Sb}$ ca. 3.5 and 4.5 Å). Each of the remaining twelve surface Cu atoms is coordinated trigonally planar by three Sb atoms and is located in the centre of the Sb_3 faces of the Sb_{16} shell. These outer three coordinate Cu atoms are also located in the centre of a trigonal face of the polyhedron formed by the sixteen $\{\text{Cu}(\text{PEt}_2\text{Me})\}$ units. The organic groups of the phosphine ligands prevent the coordination of additional phosphine ligands to the three-coordinate Cu atoms. Having solved the structure of **47** we were unable to unequivocally identify the atom type in the centre of the cluster (herein refined as Cu(6)) by crystallographic methods alone. Other analytical tools, such as elemental analysis and mass spectrometric methods, also failed to give us clear evidence. Again the accuracy of the X-ray structure determination was assessed by DFT methods. Calculations for the isomorphous cluster cores $[\text{Cu}_{40}\text{Sb}_{21}]$ (**46a**), $[\text{Cu}_{41}\text{Sb}_{20}]$, $[\text{Cu}_{44}\text{Sb}_{17}]$, and $[\text{Cu}_{45}\text{Sb}_{16}]$ with PMe_3 ligands in molecular symmetry T were performed. Figure 33 shows the deviation between measured and calculated bond lengths in **47**.

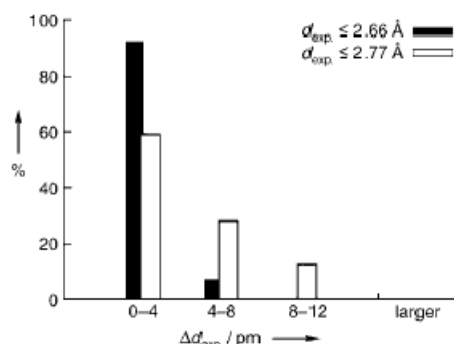


Figure 33. Deviations of selected calculated from experimentally determined metal···metal distances (d_{exp}) in 52

This deviation is most meaningful for short and strong bonds which are those described best by theory. $[\text{Cu}_{45}\text{Sb}_{16}\text{L}_{16}]$ ($\text{L}=\text{PMe}_3$) gives a perfect match: short bonds ($\leq 2.66 \text{ \AA}$) deviate by only up to 0.08 \AA , and the deviation is less than 0.04 \AA in over 90% of cases. Even for a larger cutoff, bonds $\leq 2.77 \text{ \AA}$, which includes relatively weak bonds there are no discrepancies larger than 0.12 \AA . All the calculated cluster cores contain 61 metal atoms stabilized by phosphine ligands, but for $\text{Cu}:\text{Sb} \neq 45:16$ they show unacceptably large deviations from X-ray results and can be reliably excluded. The electronic structure of **47** shows remarkable features. The odd numbers of electrons leads to an open-shell structure with a singly occupied tHOMO in molecular symmetry T resulting in a ^2T state that will undergo a (slight) Jahn–Teller distortion. The high-lying HOMO, $\epsilon_{\text{HOMO}}=-1.902 \text{ eV}$, and a band gap of 0.85 eV between HOMO and HOMO-1 indicate that **47** is a strong reducing agent. In addition to the synthesis of the molecular CuSb alloys **46** and **47**, which are nonclassical compounds in a sense that they cannot be described by localized charges, calculations of the largest CuSb clusters have shown that DFT calculations can assist in the correct assignment of atom types in highly symmetric crystal structures. It can be assumed that the synthesis of even larger CuSb alloy complexes does not simply proceed via elimination of volatile trimethylsilyl-containing leaving groups but instead via aggregates similar to **47** which could act as reducing agents in reactions with other metal cations present in solution.

From the above described combination of X-ray analysis and DFT calculation we learned that this method is a powerful tool for a better understanding of structures. A further example is the structure and characterization of **48**. The reaction of CuOAc and $\text{Sb}(\text{SiMe}_3)_3$ (ratio 1:1) in the presence of PEt_3 produces the Cu–Sb cluster $[\text{Cu}_{28}\text{Sb}_{12}(\text{PEt}_3)_{12}\{\text{Sb}(\text{SiMe}_3)_2\}_2]$ (**48**) (Scheme 10).



Scheme 11. Synthesis of **48**.

The initial X-ray structural analysis of black crystals of **48** led to problems with the atom assignment of Cu(5,10,17) and Sb(6,8,10) and their symmetry equivalents, indicated by unusual thermal parameters. All other atoms could be unequivocally identified. Figure 34 represents the refined structural model of **48** based on results obtained from DFT calculations.

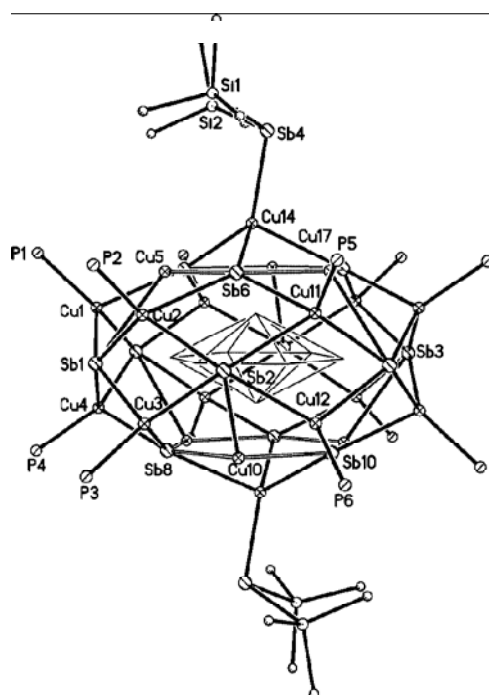


Figure 34. Molecular structure of **48**. Et groups and bonds to the inner [Cu₈] unit omitted.

The DFT study was carried out to allow reliable assignment of atom types to the positions in question [Cu(5,10,17), Sb(6,8,10) and symmetry equivalents]. All calculations were performed with the TURBOMOLE program package by employing the BP86 functional with the very efficient MARI-J approximation, and recently developed TZVP basis sets. For P–Me and –Et smaller basis sets were used. The number of contracted basis functions is as follows: Sb [6s5p3d2f], Cu [6s4p4d1f], Si [5s5p2d1f], P [5s5p2d1f], C [5s3p1d], and H [2s]. The core electrons 1s to 3d of Sb (28 electrons) were modeled by a small-core ECP (Effective Core Potential), taking into account scalar relativistic effects. The results of these calculations give a clear preference to six-membered [CuSb]₃ rings (indicated by open bonds in Figure 1) over Cu₆, Sb₆, Cu₄Sb₂, Cu₂Sb₄, and permutations thereof. [CuSb]₃ rings, however, can be in different orientations relative to each other. The calculated structures of **48** and a conformer (generated by the exchange of all Cu and Sb positions within slightly puckered six-membered rings) are equally stable ($\Delta = 4$ kJ/mol) and fit with a structure solution of X-ray crystallographic data, based on these DFT suggestions. The calculated structure of the acentric isomer of **48** is 28 kJ/mol more stable than calculated **48** but shows larger deviations of Cu–Sb bond lengths and would require lower crystallographic symmetry. Although an acentric structure of **48** was initially ruled out when refinement of a structural model in the space group $P2_1$ did not indicate a preference for Cu or Sb on any site in the highlighted six-membered [CuSb]₃ rings, the findings of DFT calculations and X-ray crystallographic results are not contradictory and point towards individual acentric cluster molecules with a 50:50 distribution. This results in a pseudo-centrosymmetric solid-state structure of **48** representing the average composition rather than an individual molecule. Based on these considerations, the structure of **48** and its conformer was solved and refined in the space group $P2_1/n$. Atomic positions within the six-membered rings were refined with 50% occupancy of both Cu and Sb. The solid-state structure of **48** (Figure 34) consists of a central hexagonal-bipyramidal arrangement of Cu atoms surrounded by a distorted icosahedral arrangement of Sb atoms and an additional layer of a capped hexagonal prism of 14 Cu atoms (Figure 35).

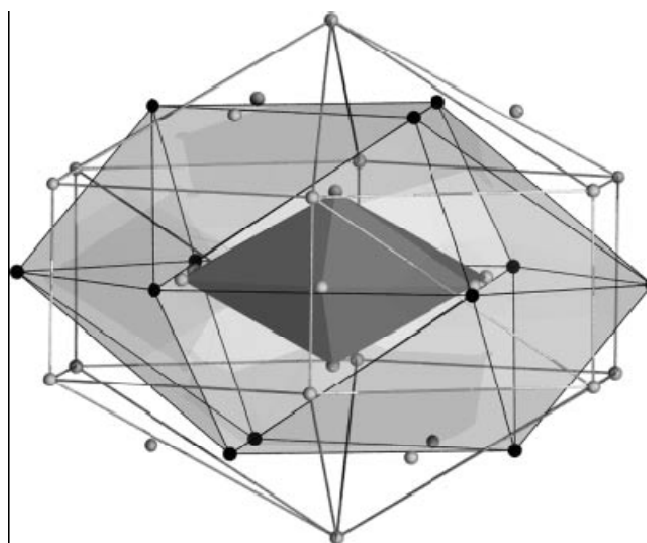
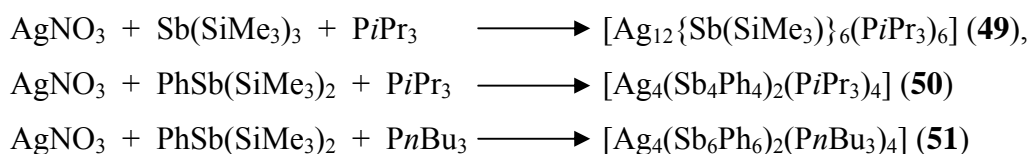


Figure 35. Polyhedral model of the cluster core found in **48** (Sb black, Cu grey).

We were also interested in the synthesis of Ag-Sb clusters [23]. In fact there are no reports about these compounds up to now. In contrast to antimony, several examples for arsenic anions bridging silver or gold centres are known.[11, 26] The silver arsinidene cluster $[\text{Ag}_{14}(\text{AsPh})_6\text{Cl}_2(\text{PEt}_3)_8]$ or the isostructural complexes $[\text{Ag}_4(\text{As}_4\text{Ph}_4)_2(\text{PEt}_3)_4]$ and $[\text{Au}_4(\text{As}_4\text{Ph}_4)_2(\text{P}n\text{Pr}_3)_4]$ can be obtained by the reaction of coinage metal salts with $\text{PhAs}(\text{SiMe}_3)_2$ in the presence of tertiary phosphanes [26]. This prompted us to attempt the synthesis of silver and gold complexes containing antimony anions. In the following first results of mixed-metal Ag/Sb complexes are described. The reactions of silver nitrate with stibanes produced the silver antimony compounds $[\text{Ag}_{12}\{\text{Sb}(\text{SiMe}_3)\}_6(\text{PiPr}_3)_6]$ (**49**), $[\text{Ag}_4(\text{Sb}_4\text{Ph}_4)_2(\text{PiPr}_3)_4]$ (**50**) and $[\text{Ag}_4(\text{Sb}_6\text{Ph}_6)_2(\text{P}n\text{Bu}_3)_4]$ (**51**) (Scheme 12).



Scheme 13. Synthesis of the Ag/Sb complexes **49**, **50** and **51**.

The complex **49** crystallizes from diethyl ether as orange blocks in the trigonal space group $P\bar{3}$ with three molecules in the unit cell. It can be described by a distorted triangular antiprism of antimony atoms in which every edge is capped by a silver atom (Ag1) (Figure 36, left). The other six silver atoms (Ag2) are coordinated by phosphane ligands. On each Sb atom a trimethylsilyl group is retained. The Sb–Ag distances in **49** are similar to reported average Ag–Sb distances of 2.72 Å in compounds with most of them of the general type $[\text{R}_3\text{Sb–AgX}]$ (R = organic group, X = anion). The stability of the cluster compounds increased when $\text{PhSb}(\text{SiMe}_3)_2$ was used as antimony source. By the reaction of AgNO_3 with $\text{PhSb}(\text{SiMe}_3)_2$ and four equivalents of PiPr_3 in diethyl ether the cluster compound $[\text{Ag}_4(\text{Sb}_4\text{Ph}_4)_2(\text{PiPr}_3)_4]$ (**50**) is obtained as red crystals together with colourless blocks of the silver phosphane complex $[\text{Ag}(\text{NO}_3)(\text{PiPr}_3)_2]$ and $[\text{PhSb}]_6$.

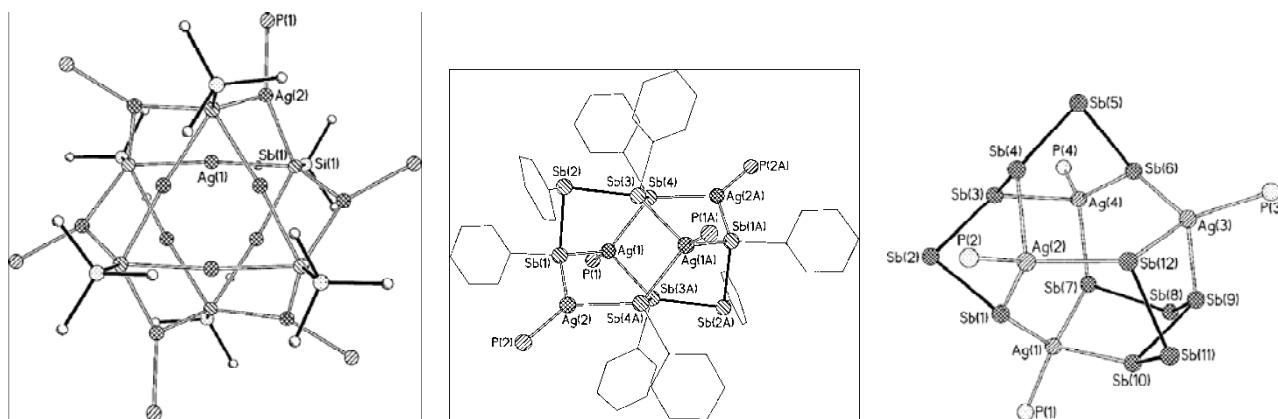


Figure 36. Molecular structures of **49** (left), **50** (middle) and **51** (right) without organic substituents.

The molecular structure of **50** (Figure 36, middle) is isostructural to the structure of $[\text{Ag}_4(\text{As}_4\text{Ph}_4)_2(\text{PET}_3)_4]$ in the solid state. The structure of **50** can be described as a centrosymmetric dimer of a $[(\text{PhSb})_4]^{2-}$ anion and two Ag-phosphane units. Each $[(\text{PhSb})_4]^{2-}$ anion chelates Ag(1,1A) by terminal Sb atoms. Ag(2) is coordinated by Sb atoms of different anions. The longest Ag–Sb bond in **50**, which is observed between Sb(3) and Ag(1A), corresponds to distances commonly observed between neutral stibanes and AgI centres. These interactions are slightly longer than bonds between silver and terminal antimony atoms. The coordination sphere of the four silver atoms is completed by additional $\text{P}i\text{Pr}_3$ ligands. The formation of the $[(\text{PhSb})_4]^{2-}$ anion in **50** is intriguing, and it is currently assumed that **50** represents an intermediate of the AgI-induced oxidation of $\text{PhSb}(\text{SiMe}_3)_2$ to *cyclo*- $[\text{PhSb}]_6$. The Sb–Sb distances are in the range of reported Sb–Sb bond lengths of about 2.8 Å. The use of the phosphane $\text{P}n\text{Bu}_3$ instead of $\text{P}i\text{Pr}_3$ leads to the cluster compound $[\text{Ag}_4(\text{Sb}_6\text{Ph}_6)_2(\text{P}n\text{Bu}_3)_4]$ (**51**). The molecular structure of **56** (Figure 36, right) consists like **50** of two *oligo*- $[(\text{PhSb})_6]^{2-}$ anions and four Ag atoms. Compound **51**, however, represents, in comparison to **50**, an intermediate where the $[\text{PhSb}]_6$ chain is preformed at metal centres and “ready to cyclize” to *cyclo*- $[\text{PhSb}]_6$, which is formed in all the investigated reactions between AgI salts and $\text{PhSb}(\text{SiMe}_3)_2$. The almost tetrahedral arrangement of the four Ag atoms in **51** is favoured by the sterically demanding anions over the centrosymmetric arrangement in the solid-state structure of **50** or other possibilities. Each of the $[(\text{PhSb})_6]^{2-}$ anions in **51** chelates two Ag atoms forming five-membered rings as observed in **50** and all Ag atoms are coordinated by Sb atoms of both dianions. Bond lengths between silver atoms and inner antimony atoms in **51** are ca. 0.2 Å longer than distances Ag–Sb(terminal).

References

- [1] S. Dehnen, A. Eichhöfer, D. Fenske, *Eur. J. Inorg. Chem.*, 279 (2002)
- [2] M.-L. Fu, I. Issac, D. Fenske, O. Fuhr, *Metal-rich Copper Chalcogenide Clusters at the Border Between Molecule and Bulk Phase – The Structures of $[\text{Cu}_{93}\text{Se}_{42}(\text{SeC}_6\text{H}_4\text{SMe})_9(\text{PPh}_3)_{18}]$, $[\text{Cu}_{96}\text{Se}_{45}(\text{SeC}_6\text{H}_4\text{SMe})_6(\text{PPh}_3)_{18}]$, and $[\text{Cu}_{136}\text{S}_{56}(\text{SCH}_2\text{C}_4\text{H}_3\text{O})_{24}(\text{dpppt})_{10}]$* , *Angew. Chem.*, **122**, 7052–7056 (2010); *Angew. Chem. Int. Ed.*, **49**, 6899–6903 (2010).
- [3] C. Cave, J. F. Corrigan, A. Eichhöfer, D. Fenske, C. M. Kowalchuk, H. Rösner, P. Scheer, *Investigation of the Thermal Properties of a Series of Copper Selenide Cluster Molecules*, *J. Cluster Science* **18**, 157 (2007)
- [4] O. Fuhr, L. Fernandez-Recio, D. Fenske, *New copper chalcogenide clusters with a selenide core and a sulfide shell*, *Eur. J. Inorg. Chem.* 230 (2005)
- [5] E. Zeller, H. Berude, A. Kolb, P. Bissinger, H. Riede, H. Schmidbaur, *Nature* **352**, 141 (1991)
- [6] D. Fenske, F. Simon, *Z. Anorg. Allg. Chem.* **622**, 45 (1996)

- [7] U. M. Tripathi, A. Schier, H. Schmidbaur, *Z. Naturforsch.* **B 53**, 171 (1998)
- [8] B. Alvarez, E. J. Fernández, M. C. Gimeno, P. G. Jones, A. Laguna, J. M. López-de-Luzuriaga, *Polyhedron* **17**, 2029 (1998)
- [9] A. L. Balch, E. Y. Fung, M. M. Olmstead, *J. Am. Chem. Soc.* **112**, 5181 (1990)
- [10] M. Richter, J. Strähle, *Z. Anorg. Allg. Chem.* **627**, 918 (2001)
- [11] P. Sevillano, O. Fuhr, M. Kattannek, P. Nava, O. Hampe, S. Lebedkin, R. Ahlrichs, D. Fenske, M. M. Kappes, *Die phosphan-stabilisierten Gold-Arsen-Cluster $[Au_{19}(AsnPr)_8(dppe)_6]Cl_3$, $[Au_{10}(AsnPr)_4(dppe)_4]Cl_2$, $[Au_{17}(AsnPr)_6(As_2nPr_2)(dppm)_6]Cl_3$ und $[Au_{10}(AsPh)_4(dppe)_4]Cl_2$ – Synthese, Charakterisierung und DFT-Rechnungen*, *Angew. Chem.* **118**, 3785–3791 (2006); *Angew. Chem. Int. Ed.* **45**, 3702–3708 (2006).
- [12] R. Ahlrichs, N. R. W. Crawford, A. Eichhöfer, D. Fenske, O. Hampe, M. M. Kappes, J. Olkowska-Oetzel, *Synthesis and Structure of Two Ionic Copper Indium Selenolate Cluster Complexes $[As(C_6H_5)_4]_2[Cu_6In_4(SeC_6H_5)_{16}Cl_4]$ and $[As(C_6H_5)_4][Cu_7In_4(SeC_6H_5)_{20}]$* , *Eur. J. Inorg. Chem.*, 345 (2006);
- [13] A. Eichhöfer, D. Fenske, J. Olkowska-Oetzel, *Synthesis and Structure of $[nPr_3N(CH_2)_6nPr_3][CuFe_3Br_3(SePh)_6]$, $[Cu_5Fe(SePh)_7(PPh_3)_4]$, and $[Cu_4Fe_3Br_3(SePh)_{10}(PPh_3)_4]$* , *Eur. J. Inorg. Chem.* 74 (2007)
- [14] P. Strickler, *J. Chem. Soc. D*, 655 (1969)
- [15] R. Ahlrichs, D. Fenske, M. McPartlin, A. Rothenberger, C. Schroth, S. Wieber, *Phosphan-stabilisierte Cu-Sb-Cluster: Synthesen, Strukturen und theoretische Untersuchungen von $[Cu_{12}(SbSiMe_3)_6(PiPr_3)_6]$, $[Cu_{40}Sb_{12}(PMe_3)_{20}]$ und $[Cu_{45}Sb_{16}(PEt_2Me)]$* , *Angew. Chem.* **117**, 4002 (2005); *Angew. Chem. Int. Ed.* **44**, 3932 (2005)
- [16] J. Lackmann, R. Hauptmann, S. Weißgräber, G. Henkel, *Chem. Commun.*, 1995 (1999)
- [17] H.-O. Stephan, G. Henkel, M. G. Kantatzidis, *Chem. Commun.*, 67 (1997)
- [18] D. Fenske, C.E. Anson, A. Eichhöfer, O. Fuhr, A. Ingendoh, C. Persau, C. Richert, *Synthesen und Kristallstrukturen von $[Ag_{123}S_{35}(StBu)_{50}]$ und $[Ag_{344}S_{124}(StBu)_{96}]$* , *Angew. Chem.* **117**, 5376–5381 (2005); *Angew. Chem. Int. Ed. Engl.* **44**, 5242–5246 (2005)
- [19] C. Anson, A. Eichhöfer, I. Issac, D. Fenske, O. Fuhr, P. Sevillano, C. Persau, D. Stalke, J. Zhang, *Synthesis and crystal structures of the ligand-stabilized silver chalcogenide clusters $[Ag_{154}Se_{77}(dppxy)_{18}]$, $[Ag_{320}(StBu)_{60}S_{130}(dppp)_{12}]$, $[Ag_{352}S_{128}(StC_5H_{11})_{96}]$, and $[Ag_{490}S_{188}(StC_5H_{11})_{114}]$* , *Angew. Chem.* **120**, 1346–1351 (2008); *Angew. Chem. Int. Ed. Engl.* **47**, 1326–1331 (2008),
- [20] X. J. Wang, T. Langetepe, C. Persau, B. S. Kang, G. S. Sheldrick, D. Fenske, *Angew. Chem.* **114**, 3971 (2002); D. Fenske, C. Persau, S. Dehnen, C. E. Anson, *Angew. Chem.* **116**, 309 (2004)
- [21] S. Chitsaz, D. Fenske, O. Fuhr, *Silberchalkogenidcluster mit Dimethylanilinmercapto-Liganden: Synthesen und Kristallstrukturen von $[Ag_{65}S_{13}(SC_6H_4NMe_2)_{39}(dppm)_5]$, $[Ag_{76}Se_{13}(SC_6H_4NMe_2)_{50}(PPh_3)_{6.5}]$ und $[Ag_{88}Se_{12}(SC_6H_4NMe_2)_{63}(PPh_3)_6]$* , *Angew. Chem.* **118**, 8224–8228 (2006); *Angew. Chemie. Int. Ed. Engl.* **45**, 8055–8059 (2006)
- [22] R. Ahlrichs, D. Fenske, M. McPartlin, A. Rothenberger, C. Schroth, S. Wieber, *Phosphan-stabilisierte Cu-Sb-Cluster: Synthesen, Strukturen und theoretische Untersuchungen von $[Cu_{12}(SbSiMe_3)_6(PiPr_3)_6]$, $[Cu_{40}Sb_{12}(PMe_3)_{20}]$ und $[Cu_{45}Sb_{16}(PEt_2Me)]$* , *Angew. Chem.* **117**, 4002–4005 (2005); *Angew. Chem. Int. Ed.* **44**, 3932 (2005); R. Ahlrichs, D. Fenske, A. Rothenberger, C. Schroth, S. Wieber, *Atom Assignment in Solid-State Structures on the Basis of X-ray Crystallography and DFT Calculations – A Case Study on a Molecular Cu-Sb Alloy*, *Eur. J. Inorg. Chem.* 1127 (2006)
- [23] D. Fenske, A. Rothenberger, S. Wieber, *Synthesis and Characterization of the First Silver Complexes with Antimony Anions*, *Eur. J. Inorg. Chem.* 648–651 (2007)

- [24] J. Besinger, J. Treptow, D. Fenske, *Z. Anorg. Allg. Chem.* **628**, 512 (2002); D. Fenske, A. Rothenberger, S. Wieber, *Z. Anorg. Allg. Chem.* **629**, 929 (2003); R. Ahlrichs, C. E. Anson, R. Clerac, D. Fenske, A. Rothenberger, S. Sierka, S. Wieber, *Eur. J. Inorg. Chem.*, 2933 (2004)
- [25] ASM Speciality Handbook, Copper and Copper Alloys (Eds. J. R. Davis), Davis & Associates, ASM International 2001
- [26] D. Fenske, F. Simon, *Z. Anorg. Allg. Chem.* **622**, 45 (1996); D. Fenske, W. Holstein, *Angew. Chem.* **106**, 1311 (1994); *Angew. Chem. Int. Ed.* **33**, 1290 (1994); J. Besinger, D. Fenske, *Z. Anorg. Allg. Chem.* **627**, 1487 (2001)